FINNISH METEOROLOGICAL INSTITUTE
CONTRIBUTIONS

No. 30

SWAN LYMAN ALPHA IMAGER COMETARY HYDROGEN COMA OBSERVATIONS

J. Teemu T. Mäkinen

DISSERTATION

To be presented, with the permission of the Faculty of Science of the University of Helsinki, for public criticism in Auditorium XIV of the main building on June 8, 2001, at 12 o'clock.

Finnish Meteorological Institute
Helsinki 2001

ISBN 951-697-540-2 (PB)
ISBN 951-45-9981-0 (PDF)
ISSN 0782-6117

Yliopistopaino
Helsinki 2001

FINNISH METEOROLOGICAL INSTITUTE

Published by Finnish Meteorological Institute
Vuorikatu 24, P.O. Box 503
FIN-00101 Helsinki, Finland

Series title, number and report code of publication
Contributions 30, FMI-CONT-30

Date
May 2001

Authors
J. Teemu T. Mäkinen

Name of project

Commissioned by

Title
SWAN Lyman alpha imager cometary hydrogen coma observations

Abstract

This thesis consists of an introductory section and five original research papers. The work deals with two different applications of the SWAN (Solar Wind ANisotropies) Lyman α imager instrument in connection with cometary studies: detecting comets and estimating their water production rates. This is possible because the extended hydrogen coma of an active comet resonantly scatters solar ultraviolet light.

The SWAN instrument onboard the SOHO (Solar and Heliospheric Observatory) spacecraft is capable of imaging the entire sky on a daily basis. A neural network was developed to search the SWAN database for comets (paper 2). This resulted in the late discovery of one moderately bright comet which had not been detected during its apparition (paper 1). Furthermore, an in-depth survey of the database revealed that it contained pre-discovery observations of about half of the new bright comets (paper 3). This has demonstrated the feasibility of SWAN-type monitoring of new comets, which – together with asteroids – pose the most tangible long term threat to the existence of mankind.

Water is the dominant volatile component of comets. Accurate measurements of the water production rate of a comet give an estimate of the size, dynamics and sometimes even of the rotational state of the cometary nucleus. Robust estimates are especially important for comets which are targets of near-term space missions, like comets Encke and Wild 2 (paper 4). Furthermore, a complete disintegration of a comet made it possible to observe its internal structure (paper 5).

The introductory part provides the proper context for the research papers, describing cometary water production observations in general and reviewing the physical phenomena affecting the hydrogen coma, and suggests new research initiatives.

Publishing unit
Geophysical Research

Classification (UDK)
520.6.05:520.624–74, 523.64–126, 523.64–44, 523.64–857:520.82.054–74

Keywords
comets, ultraviolet observations, survey, water production

ISSN and series title
0782-6117 Finnish Meteorological Institute Contributions

ISBN
951-697-540-2 (PB) 951-45-9981-0 (PDF)

Language
English

Sold by
Finnish Meteorological Institute / Library
P.O.Box 503, FIN-00101 Helsinki
Finland

Pages 134

Price

Note

Preface

This thesis is based on work performed at the Geophysical Research Division (GEO) of the Finnish Meteorological Institute (FMI) and funded by the Academy of Finland. The objective of the work has been to utilize the wealth of cometary data obtained with the SWAN (Solar Wind ANisotropies) instrument on board the SOHO (SOlar and Heliospheric Observatory) spacecraft as a byproduct of its primary scientific objective of determining the distribution of interplanetary neutral hydrogen from sustained observations at the ultraviolet Lyman alpha wavelength. Since this spectral range is not available for ground-based observations, the SWAN data form a unique set which produces valuable new information as demonstrated by the five original papers which, together with this introductory part, form a Ph.D. thesis:

1. Mäkinen, J.T.T., J.L. Bertaux, H. Laakso, T. Pulkkinen, T. Summanen, E. Kyrölä, W. Schmidt, E. Quémerais and R. Lallement, 2000. Discovery of a comet by its Lyman-α emission. *Nature* **405**, 321–322.

2. Mäkinen J.T.T., M.T. Syrjäsuo and T.I. Pulkkinen, 2000. A Method for Detecting Moving Fuzzy Objects from SWAN Sky Images. In *Proceedings of the IASTED International Conference, Signal and Image Processing*, M. H. Hamza, ed., pp. 151–154.

3. Mäkinen J.T.T., J.L. Bertaux, T.I. Pulkkinen, W. Schmidt, E. Kyrölä, T. Summanen, E. Quémerais and R. Lallement, 2001. Comets in full sky L_α maps of the SWAN instrument. I. Survey from 1996 to 1998. *Astron. Astrophys.* **368**, 292–297.

4. Mäkinen J.T.T., J. Silén, W. Schmidt, E. Kyrölä, T. Summanen, J.L. Bertaux, E. Quémerais and R. Lallement. Water Production of Comets 2P/Encke and 81P/Wild 2 Derived from SWAN Observations During the 1997 Apparition. *Icarus*, in print.

5. Mäkinen, J.T.T., J.L. Bertaux, M.R. Combi and E. Quémerais. Water Production of Comet 1999 S4 LINEAR Observed with the SWAN

Instrument. *Science*, in print.

The introductory part is divided into four chapters describing cometary science in general, observational aspects, models for the neutral coma and near-term SWAN-related initiatives, respectively. The first chapter is written to be accessible to larger audiences whereas the remaining three chapters assume the reader to have a basic understanding of physical sciences. Furthermore, the fourth chapter very briefly describes several topics with the implication that a full treatment will be given in due time as related projects mature.

The first three research papers deal with the aspects of SWAN as a survey instrument. As shown in the third paper which reviews the survey project conducted on the "classical data set", i.e., the data gathered before the June 1998 loss of SOHO for a period of three months, half of the bright new comets appearing during the SWAN operating period were visible on SWAN sky maps before their actual discovery date. The amount of prediscovery observations varies from some days to several months worth of recorded activity. This is not, however, a manifestation of the superior resolving power of the instrument which, with one square degree pixels and very modest sensitivity, is in this respect inferior to most amateur telescopes. Instead, the success of SWAN relies on the advantage of repeated observations with very large coverage, and on digital image manipulation. The second paper thus describes the image processing method that was developed to detect comets automatically from full sky maps. Although comparable methods have been applied elsewhere, the specific issues with SWAN data required a customized solution. The late discovery of a comet as presented in the first paper might by itself not strike one as a very remarkable result, especially since the comet in question did not display any extraordinary activity. The notion that a relatively bright comet may pass by unnoticed is, however, discomforting when the possible implications are considered.

The fourth and fifth papers concentrate on another aspect of SWAN observations — the ability to derive the water production rate of a comet in a systematic and consistent manner regardless of the position of the

comet, all the way to the immediate vicinity of the Sun. The two short-period comets discussed in the fourth paper are targets of near-term space missions and publishing the data in their current state brings valuable new information to the groups preparing for these missions. Furthermore, GEO is part of both these upcoming missions and since the division has the necessary knowledge for getting involved with all the aspects of the cometary coma — dust, neutral gas and plasma and fields — research synergies can be anticipated to produce tangible results in the future. The fifth paper deals with the serendipitous break-up of a comet near its perihelion passage. The comet was bright enough for an excellent set of observations to be made, which yielded some fundamentally important insights. When comparing the scientific significance of the presented papers, the first and fifth paper may both be quite profilic but where the first paper could be seen as a strike of good luck, perhaps helped a little by clever image manipulation, the results of the fifth paper were obtained through the application of a sound physical framework.

Since these papers are contained in a thesis, it is necessary to mention the personal contributions of the author. The realization and operation of the SWAN instrument and the related software is an effort of the SWAN team at FMI and Service d'Aéronomie (SA), France. The decision on the type of model used to estimate water production rates was made by the principal investigator of the SWAN instrument, Dr. Jean-Loup Bertaux, at SA. The author himself is responsible for programming the model as well as various other utilities mentioned in Appendix B. The papers represent personal work of the author where, the fifth paper notwithstanding, outside contribution was restricted to professional insights at the manuscript writing phase given by Dr. Harri Laakso and Mr. Mikko Syrjäsuo for the first and second papers, respectively. The fifth paper was written in closer co-operation with Dr. Michael Combi and Dr. Jean-Loup Bertaux where the author is responsible for the data processing and about two thirds of the written material. The draft was also seen and discussed by the team coordinator of the special issue, Dr. Harold Weaver, before submission. Also, for all the papers, many useful suggestions were made by many other colleagues as well as by the referees of the papers.

This work would not have been possible without the direct or indirect influence of many people whom I can only mention some here. I want to express my sincere gratitude to the head of the division, Prof. Risto Pellinen, for providing the working environment and necessary facilities, to my supervisor, Prof. Tuija Pulkkinen, for her prompt and practical advice and continuing support during this project and to the head of space physics group, Dr. Risto Pirjola, for initially taking me into the division, trusting my abilities enough to give me free hands to pursue my own research initiatives, and providing opportunities to reflect new ideas. I want to thank the SWAN team and especially Dr. Jean-Loup Bertaux, for providing support and insights. The coauthors and referees of my papers must also be given their due acknowledgements for intelligent and constructive correspondence, and furthermore, I am thankful to the whole personnel of GEO for creating a great working atmosphere. Among all the encouraging colleagues special thanks must be addressed to the space technology coordinator of GEO, Mr. Ari-Matti Harri, who has periodically reminded me that a Ph.D. thesis should not be the culmination of a scientist's career, and considering that this work is now here, the message seems to have finally sunk in. In the practical art of using LaTeX I am in debt for Dr. Tero Siili for his indispensable recommendations. I am also grateful to composer Karl Jenkins whose Adiemus music has inspired me during the long and lonely working sessions needed to get this thesis done. Last but not least, thanks are also due to my wife Teija whose efforts on the laundry, dinner and dishes department have enabled me to complete this work in time and relatively free of earthly concerns.

Contents

Chapter 1

Introduction

1.1 Historical perspective

The word comet comes from the Greek language ($\kappa o \mu \acute{\eta} \tau \eta \varsigma < \kappa \acute{o} \mu \eta$, *lit. hair*). This is a reference to the distinguishing feature of comets, the dust tail that forms as the solar radiation pressure pushes away small particles released by the comet near perihelion when heated ice evaporates from the surface. In other languages this ephemeral phenomenon has coined names as varied as "tail stars", "broom stars" or even "smoking stars". While the periodicity of most celestial phenomena including solar and lunar eclipses were known to the ancients, the rare and irregular appearances of comets combined with their peculiar nature gave rise to many superstitious beliefs. In the Middle Age Europe comets were seen as bad omens, signalling times of war and pestilence. Although the influence of astrology on the decisions of contemporary leaders has hopefully diminished since then, oddly enough the combination of comets and biological agents has inspired some resonant suggestions even these days (Hoyle and Wickramasinghe, 1981).

1.1.1 Early advances

Comets were known to ancient people like the Egyptians and Babylonians but little is known about their understanding of the phenomena in

question. The Greek philosopher Aristotle taught, based on somewhat deficient reasoning, that comets were a form of weather, hot gases rising from volcanoes or the like, and catching fire as they reached the realm of heavens. Although Aristotle's arguments were already shown to be lacking by the Roman scholar and statesman Seneca living during the first decades A.D., the misconception was widely adopted until finally put to rest by the Danish astronomer Tycho Brahe whose parallax observations of the great comet of 1577 relocated comets firmly in the translunar space. That way comets became a real nuisance for the prevailing worldview, since their trajectories did not seem to pay due respect to the celestial spheres — indeed, comets blazed quite happily through the firmament as if the heavenly crystal spheres were not there at all.

Taking a short sidestep to the area of cosmogony, it must be remembered that Nicolaus Copernicus had already contested the Ptolemaic order in his 1543 work *De Revolutionibus Orbium Coelestium* but age-old beliefs were hard to turn over. Johannes Kepler worked hard in support of the Copernican model, publishing two laws of planetary motion in his 1609 work *Astronomia Nova*, and later a third one which together gave much credence to the heliocentric view. Galileo Galilei was aware of Kepler's work and he went on to challenge the Catholic church with well-known consequences. It is less well known, however, that Galilei used faulty reasoning of his own to argue in favour of a moving Earth and that the controversy had more to do with personal issues than a confrontation between the church and science, as it is often portrayed.

At the same time, the origin, nature and orbital characteristics of comets were hotly debated. It was suggested that comets were ejected splinters from other planets like Jupiter, and that they rushed through the solar system on straight lines. It was through the collaboration of two prominent English scientists, Isaac Newton and Edmond Halley, that comets finally came to receive their place among other bodies of the solar system. Prompted by Halley, Newton (1687) proved that the laws of Kepler follow from the assumption of a universal force of gravity which decreases as the inverse square of distance. Furthermore, Halley noticed similarities in the orbital parameters of the comets of 1531, 1607 and 1682, and in

1705 made a far-sighted prediction: all these were apparitions of just one periodic comet which would return at the end of 1758. He even gave the orbital elements for that apparition and told from which part of the sky the comet could be expected to arrive. Closer to the time of return Halley's calculations were revised by three French scientists, Joseph Lalande, Alexis Clairaut and Nicole-Reine Lepaute. They found out that Halley had made some errors which nearly compensated each other so that the result did not change too much. Halley's prediction was finally proven true long after his death by a German amateur astronomer on Christmas night, 1758, when he found the comet now named in honour of this remarkable scientist in the exact place Halley had predicted.

Another fundamental insight about cometary orbital dynamics was conceived soon thereafter. The French astronomer Charles Messier had found a new comet on June 14, 1770, while observing Jupiter. He then continued systematic observations until October 3 the same year, when the comet could be resolved the last time ever. In 1776 the Finnish astronomer Anders Lexell suggested that the comet had had a close encounter with Jupiter which had injected the comet into an elliptic orbit with a period of 5.6 years. Furthermore, a second encounter with Jupiter ejected the comet out of the inner solar system again. Because the comet had not perturbed the orbits of the satellites of Jupiter, it had to have very little mass. The comet, known today as D/1770 L1 Lexell, was not just the first documented example of chaos in orbital mechanics, but it also made to date the closest known cometary encounter with the Earth, missing a direct hit by a mere 0.0151 AU on July 1, 1770.

The question of the nature of comets still remained. Newton had shortly discussed the topic in his *Principia*, inferring the existence of a small solid nucleus as the source of the visible tail. He also identified solar heating as the cause of emission of the fine vapour constituting the tail. The Prussian philosopher Immanuel Kant came very close to the right answer by reasoning that comets formed in the farthest reaches of the universe and because they often become active beyond the distance of the orbit of the Earth, they must be made of some very light substance. Pierre Simon, Marquis de Laplace, was on the same lines, and he also identified Jupiter's gravitational

influence as an explanation for the observed properties of different families of comets. Kant and Laplace are also given credit for suggesting the solar nebula hypothesis, whose basic idea of the origin of the solar system has later been proved correct. Still all of those great scientists refrained from stating what in hindsight seems almost obvious — that the extremely light substance of comets is ordinary and ubiquitous water ice.

More clues about the composition of comets were obtained after the association between meteor showers and comets was found by the Italian astronomer Giovanni Schiaparelli who identified the Perseid meteor shower with the comet 109P/Swift-Tuttle. In a program guided by Donald Brownlee, particles small enough to decelerate without melting upon arrival to the atmosphere have been collected from the stratosphere and brought to laboratories for further inspection. These particles are fluffy aggregates of minerals and organics — the residual dust void of volatiles (Brownlee, 1979). For a considerable time, comets were seen as celestial hail storms, a swarm of small particles on parallel orbits. This was still suggested fairly recently by Lyttleton (1948, 1953) with his "sand bank" model. Contrary evidence, however, continued to pile up and prompted Whipple (1950, 1951) to propose the "dirty icy ball" model, which has been proven to be essentially correct by later observations. Comets may, however, be a more diverse lot than originally expected, and some revisions may be needed as new evidence comes in.

It must be understood that the given account of events is decidedly biased towards the European point of view. On a purely observational basis, the meticulous work of Chinese, and to some extent Korean and Japanese, astronomers through centuries was far superior to their western counterparts' sporadic efforts and the Chinese astronomical records are still a valuable source of information. But although the Chinese even composed the world's first cometary atlas, known from the *Mawangdui silk* from around 300 B.C., whereabouts of comets and other celestial phenomena were closely guarded secrets of state and the emperor's celestial counselors, in the pragmatic tradition of the Chinese science of the time, apparently never pondered the actual nature of comets.

1.2 Recent contributions

According to current understanding, comets are solid bodies consisting mainly of water ice and non-volatile dust in roughly equal proportions, and represent the least reprocessed matter originally condenced in the presolar nebula. The two main reservoirs of comets are the Kuiper belt (Kuiper, 1951) beyond the orbit of Neptune and the Oort cloud (Oort, 1950) created from primordial bodies scattered by the gravitational perturbation by giant planets, which, with its outer range at about 10^5 AU represent the outermost extension of the solar system. While normally inactive bodies, some comets are transferred to orbits with small perihelion distances by perturbations caused by the giant planets, passing stars and molecular clouds, and galactic tides. Near the Sun, cometary matter evaporates forming a tenuous atmosphere known as a "coma" with dust and plasma tails.

1.2.1 Space missions

Remote observations must be supported by *in situ* measurements for a complete picture of cometary physics and chemistry to emerge. This phase of exploration began with close cometary encounters pioneered by an unlikely attendant. A near-Earth spacecraft known as *International Sun-Earth Explorer 3* (ISEE 3) was recycled after its nominal end of mission by an ingenious series of lunar gravity assists which took it to the vicinity of the comet 21P/Giacobini-Zinner on September 11, 1985. The spacecraft, renamed *International Cometary Explorer* (ICE) (Brandt and Niedner, 1985), flew through the tail of the comet, discovered that the interplanetary magnetic field was draped over the nucleus and witnessed unexpected high-energy particles and field events in the tail. At the end of March 1986 ICE flew past comet 1P/Halley at a distance of 28 million km.

The 1986 apparition of 1P/Halley was greeted with six other spacecraft, as well. Besides another recycled spacecraft, *Pioneer 7*, which reached a distance of 12 million km from the nucleus, these included the Japanese *Sakigake* (pioneer) and *Suisei* (comet) (Oya, 1986), the Soviet *Vega 1* and *2* (Grard *et al.*, 1986) (after the Russian pronounciation of Venus–Halley)

and the European *Giotto* (Lo Galbo, 1984) (after an Italian painter who used the 1301 apparition of comet Halley in the background of a fresco). Sakigake was a kind of a reference platform which never came closer than 7 million kilometers away from the nucleus. Suisei reached the distance of 1.5×10^5 km and carried a UV camera for observations of the hydrogen coma. The Vega 1 and 2 spacecraft both passed the nucleus at a distance of about 1×10^4 km on 6 and 9 March 1986, respectively, and through an exemplary event of international cooperation their observations were used to fine-tune the trajectory of Giotto to pass the daylight side of the nucleus on March 13, 1986, at a distance of only six hundred kilometers. Although Giotto was temporarily knocked astray by debris during the closest encounter, it managed to record a magnificent set of images which at last revealed the eluding entity, the irregular and dark nucleus which is the comet proper. Afterwards, Giotto was retargeted to encounter a less profilic comet, 26P/Grigg-Skjellerup in July 1992 (Schwehm, 1992).

The combined Halley missions, supported by a variety of remote sensing efforts, were a great success, yielding one discovery after another, and the collected data are largely responsible for our current view of comets. Some of the most important advances in our understanding of comets include the confirmation of a solid, irregularly shaped nucleus of mainly water ice with small bulk density covered by a mantle of dust with a very low geometric albedo and a random distribution of small active areas acting as sources of dust and gas jets. Also the dust composition and size distribution and the large contribution of organic matter, neutral and ion species abundances, velocities and temperatures as well as existence of CN spiral jets and the global morphology of cometary atmosphere and magnetosphere with two magnetic lobes and an ionopause, among others, were results greeted with great enthusiasm.

1.2.2 Objectives of cometary research

The current state of cometary research is most intriguing. The wealth of in situ data obtained during the first close encounters with the comets 1P/Halley and 21P/Giacobini-Zinner have been digested and exciting new

missions are under way. Still many fundamental questions about the origin, evolution, distribution and physical and chemical characteristics of comets remain open. Cometary research has also immediate and important consequences in many other fields of study as well as implications beyond pure scientific interest. In more ways than just one comets are intricately intertwined with life sciences issues. It has been suggested that we owe our very existence to cometary bodies of the solar system, and it is also well within the bounds of possibility that unless we actively work to prevent it, a comet may bring with it the eventual demise of humankind. At least the following four important reasons can be given to motivate the ongoing studies of comets.

Primordial matter

Comets consist of the most pristine material condensed in the solar nebula. Therefore their composition gives important clues to the conditions of the accretion disk. One must, however, realize that comets are not perfect time capsules — their structure and composition also evolves over timescales of millions of years. Internal heating by decay of radionuclides like ^{26}Al may have temporarily melted H_2O or at least transformed it from amorphous to crystalline state (Wallis, 1980) and caused chemical differentiation by driving outwards such highly volatile components as CO and N_2. Depending on the perihelion distance of a comet, periodic solar heating may also initiate a series of inward progressing phase transitions, likewise depleting the surface of the most volatile components. Even in the Oort cloud comets are exposed to cosmic rays which since the formation of comets may have radically altered the composition of their surface layer (Ryan Jr. and Draganić, 1986). An unstable crust could thus have formed which would explain the unusually early onset of cometary activity observed with some new comets (Johnson *et al.*, 1987).

Volatile contribution

The planets of the solar system display a clear dichotomy with the rocky inner planets from Mercury to Mars and mainly gaseous outer planets from Jupiter to Neptune. This reflects the conditions in the presolar nebula. The planetesimals that accreted to form the primordial Earth were already degassed because of the high local temperature, reaching about 700 K (Cameron, 1978) and what volatiles may have survived were subsequently vaporized in high energy impacts, especially the one which led to the formation of the Moon (Cameron, 1986). Therefore, the current volatiles must have been brought in later. As reviewed extensively by Delsemme (2000), a large body of evidence from cratering records on the Moon, Mars and Mercury to terrestial abundance ratios of various elements including isotopes of hydrogen, krypton and xenon points to comets as the source of practically all the elements that make the existence of life on Earth possible. This has an important implication for the search of habitable extrasolar planets, since similar inward transfer of volatiles will not take place in systems without massive outer planets capable of perturbing the material away from the ice condensing region.

Organic compounds

Giant molecular clouds have been found to contain a wide variety of organic molecules (Irvine and Knacke, 1989). Likewise, organic radicals such as C_2, C_3, CH and CN can be seen in the spectra of comets. They are dissociation products of complex organic compounds, collectively called "CHON" particles also detected *in situ* in 1P/Halley (Kissel and Krueger, 1987a,b), which comprise over 10% of the mass of the nucleus and are responsible for the low albedo of cometary nuclei. The organics can be of interstellar origin, produced by various reactions in the solar nebula, or directly on the comet due to cosmic radiation. Sufficiently large comets may have maintained a liquid core long enough for life to arise (Irvine *et al.*, 1980). Although the topic remains controversial, and organic compounds are prone to become pyrolyzed in a collision with a planetary body (Chyba, 1991), the organic

material covering the surface of the Earth seems to be, like volatiles, of cometary origin.

Impact hazards

The potentially devastating effect of asteroid and cometary impacts on the ecosystem of the Earth is already common knowledge. The terrestial cratering record has revealed major impacts coinciding with global mass extinctions (Alvarez *et al.*, 1980) like the Chicxulub impact basin near the Yucatan peninsula which has been connected with the Cretaceous/Tertiary boundary about 65 million years ago (Hildebrand *et al.*, 1991). More recently, a small fragment, possibly originating from the comet 2P/Encke (Kresák, 1978; Asher and Steel, 1998), caused the 1908 Tunguska event (Krinov, 1963). Also, in 1989, the Apollo asteroid 4581 Asclepius passed by the Earth at a distance closer than the Moon. The discomforting part is that it was only discovered by the *Spacewatch* survey shortly after the closest approach.

Chapter 2

Observing comets

This work concentrates on one specific ultraviolet wavelength known as the neutral hydrogen (H I) Lyman alpha (L_α) line at 121.6 nm. This particular emission line is very useful for estimating the cometary water production rate because H_2O is by far the most abundant parent molecule of H in the photodissociation process either directly or through the OH radical. Since this wavelength is completely obstructed by the atmosphere of Earth, the measurements rely on observations made with sounding rockets and satellites. The water production rate of a comet in turn is one of the most important parameters available, giving clues to the size, rotational state and surface conditions of a comet. Furthermore, H_2O forms the bulk of cometary matter to which the abundances of other species are compared.

2.1 UV experiments

The cometary L_α emission was first suggested by Biermann and Trefftz (1964) and Biermann (1968), and the first direct observation of the central region of the coma of the comet C/1969 T1 Tago-Sato-Kosaka was made on January 14, 1970, with the *Orbiting Astronomical Observatory 2* (OAO-2) satellite (Code *et al.*, 1970) and a faint and slightly defocused observation of the same comet was taken with an objective-grating spectrograph

aboard an *Aerobee* sounding rocket (Jenkins and Wingert, 1972). Later in 1970, the comet C/1969 Y1 Bennett was observed with OAO-2 (Code *et al.*, 1972; Code and Savage, 1972) and with a L_α photometer on board the *Orbiting Geophysical Observatory* (OGO-5) spacecraft (Bertaux and Blamont, 1970). These were the first observations to reveal the true extension of the hydrogen coma. OGO-5 was also used to observe the comet 2P/Encke in December, 1970 (Bertaux *et al.*, 1973). The early observations were later reviewed by Keller (1976).

The comet C/1973 E1 Kohoutek was anticipated to become one of the brightest comets of the century and an extensive observing campaign was launched. Although the comet fell far short of expectations, several L_α observations were conducted with different instruments, including sounding rockets (Opal *et al.*, 1974; Feldman *et al.*, 1974; Carruthers *et al.*, 1974; Opal and Carruthers, 1977a) and an electrographic camera on board the orbiting *Skylab* laboratory (Meier *et al.*, 1976), which provided the first direct L_α images of the hydrogen coma. Furthermore, the comet was observed by a spectrograph on Skylab (Keller *et al.*, 1975), a spectrometer aboard the *Copernicus* (OAO-3) satellite (Drake *et al.*, 1976) and another spectrometer aboard the *Mariner 10* deep space probe (Kumar *et al.*, 1979) which was the first experiment free of the Earth's exospheric L_α contribution. Sounding rocket and Skylab data were later reanalyzed by Meier *et al.* (1976). Comet Kohoutek marked the first time when high-resolution imagery and spectra became available, and also the first time when the evolution of the hydrogen coma could be observed over extended periods.

Later in the 1970s the comet C/1975 V1 West was observed with a sounding rocket (Opal and Carruthers, 1977b; Feldman and Brune, 1976) and with Copernicus (Festou *et al.*, 1983) which also observed the comets C/1975 N1 Kobayashi-Berger-Milon (Festou *et al.*, 1979) and 6P/d'Arrest (Festou *et al.*, 1983). The launch of the *International Ultraviolet Explorer* (IUE) satellite in January 1978 started the era of routine observations of cometary UV spectra, and after the first IUE observations of comet C/1978 T1 Seargent (Jackson *et al.*, 1979) and comet C/1979 Y1 Bradfield (Feldman *et al.*, 1980) many others followed. As more comets were observed it soon became apparent that cometary spectra were remarkably similar

(Weaver *et al.*, 1981). IUE remained operational until September 1996 and made a huge contribution to cometary UV studies.

The next phase in L_α observations commenced with the *Pioneer Venus Orbiter* (PVO) (Combi *et al.*, 1986) and IUE (McFadden *et al.*, 1987; Combi and Feldman, 1992) observations of 21P/Giacobini-Zinner which coincided with the comet flyby by the ICE spacecraft. This could be seen as a prelude for the 1P/Halley campaign. As mentioned earlier, of the seven spacecraft approaching the comet the Japanese Suisei had an on board UV camera (Kaneda *et al.*, 1986), and the Vega spacecraft also carried a three channel spectrometer (TKS) (Grard *et al.*, 1986). In addition, UV spectra were obtained with sounding rockets (McCoy *et al.*, 1992; Woods *et al.*, 1986), IUE (Festou *et al.*, 1986; Feldman *et al.*, 1987) and *ASTRON* (Boyarchuk *et al.*, 1986, 1987), and L_α imaging was conducted with rockets (McCoy *et al.*, 1992), PVO (Stewart, 1987) and the *Dynamics Explorer-1* (DE-1) satellite (Craven *et al.*, 1986; Craven and Frank, 1987). This was the first and to date also the only time when remote observations could be compared to *in situ* measurements.

The remarkable *Hubble Space Telescope* (HST) orbital platform has carried several UV instruments since its deployment in April 1990. The original configuration included three instruments used for cometary UV observations: the *Faint Object Spectrograph* (FOS) at 115–800 nm, the *Goddard High Resolution Spectrograph* (GHRS) at 115–320 nm and the first *Wide Field Planetary Camera* (WFPC-1) with several filters down to 115 nm. WFPC-1 was replaced by its successor, WFPC-2, on the first service mission in December 1993 and FOS and GHRS were removed on the second service mission in February 1997. Their place was taken by the *Space Telescope Imaging Spectrograph* (STIS) which has a lower limit of 115 nm as well. The problem with HST comet observations is that because of the very high usage of the platform, observing time should be reserved well in advance and thus it is very difficult to conduct a good observing program for a new comet appearing without prior notice.

2.2 Related observations

Although cometary water production rates Q_{H_2O} are in this work only discussed in the context of L_α observations, there exist many other, independent means of obtaining Q_{H_2O}. Some of these are even accessible for ground-based observers but such observations are often hampered by lack of good observing conditions or large inherent error margins. The ability to determine Q_{H_2O} from the ground is, however, an important addition to cometary studies, since continuous existence of suitable orbital facilities cannot be guaranteed in the long run. In this respect the different methods can be seen as complementary to each other and a short summary of available options is given here.

Besides the H I L_α line other UV fluorescence lines that can be used to estimate Q_{H_2O} are the O I ($^3S - ^3P$) transition line at 130.4 nm and the three OH ($A^2\Sigma^+ - X^2\Pi$) vibrational bands at 282.0 nm, 308.5 nm and 311.5 nm for the (1-0), (0-0) and (1-1) transitions, of which the 308.5 nm band is by far the most prominent. Another useful mechanism for Q_{H_2O} estimation is the "prompt emission", in which a particular species is formed directly in a metastable level from which it can then spontaneously decay. Observations of such forbidden lines tell directly the production rate of the species in question. Atomic oxygen has forbidden transitions at 297.3 nm ($^1S - ^3P$), 557.7 nm ($^1S - ^1D$), 630.0 nm and 636.3 nm ($^1D - ^3P$) of which the last two are most commonly used.

In the near infrared region H_2O has the ν_3 transition around 2.66 μm which was detected from *Kuiper Airborne Observatory* (KAO) pre-perihelion observations of comet 1P/Halley (Mumma *et al.*, 1986) and post-perihelion observations from KAO (Weaver *et al.*, 1986) and VEGA (Moroz *et al.*, 1987; Combes *et al.*, 1986). This allowed for the first time direct remote observation of H_2O itself. OH can also be observed at the fundamental (1,0) vibration band (2.80 μm) although in this context its abundance is of secondary importance. More recently new data were produced by the *Infrared Space Observatory* (ISO) (Crovisier *et al.*, 1997) which was operational between November 1995 and April 1998.

Radio wavelengths are yet another region where abundances of molec-

ular species can be observed through rotational or hyperfine transitions. These arise as a result of shorter wavelength excitations, like the well known OH $X^2\Pi_{3/2}J = 3/2$ Λ-doublet with four transitional lines at 1612 MHz, 1665 MHz, 1667 MHz and 1721 MHz which are governed by the excitation and subsequent near UV decay of the $A^2\Sigma$ state. This emission was first observed in C/1973 E1 Kohoutek (Biraud *et al.*, 1974; Turner, 1974). H_2O itself has several transitions in the centimeter to submillimeter range of which the 22.2 GHz ($6_{16} - 5_{23}$), 183 GHz ($3_{13} - 2_{20}$) and 380 GHz ($4_{14} - 3_{32}$) emissions had been monitored in the past but results were less than convincing (Crovisier and Schloerb, 1991). The new *Submillimeter Wave Astronomy Satellite* (SWAS) has finally produced an unambiguous detection of the ortho-water ($1_{10} - 1_{01}$) transition at 557 GHz (Neufeld *et al.*, 2000).

It is, of course, not necessary to restrict oneself to neutral species. The H_2O^+ 6-0 band at 700 nm was already chosen for the *International Halley Watch* (IHW) standard filter set (Osborn *et al.*, 1990) and used, e.g., by DiSanti *et al.* (1990) but the derived Q_{H_2O} rates have — because of model-related difficulties — had poor agreement with values obtained from other kinds of observations (Wegmann *et al.*, 1999).

2.3 SWAN

The *Solar and Heliospheric Observatory* (SOHO) at the first Lagrangian point about 1.5 million kilometers away from the Earth towards the Sun features a diverse combination of instruments observing solar structure and dynamics. Counterintuitively, one of the instruments is looking everywhere else except to the Sun: SWAN (Solar Wind Anisotropies) (Bertaux *et al.*, 1995) does not, despite its acronym, have anything to do with the Swan system of the C_2 radical. SWAN is a L_α imaging instrument which produces full sky UV images on a regular basis. The Sun is moving through a small galactic molecular cloud, about one parsec in diameter, known as the *Local Interstellar Cloud* (LIC) (Linsky *et al.*, 1993; Lallement *et al.*, 1994) and with a number density of about 0.15 hydrogen atoms per cm^3.

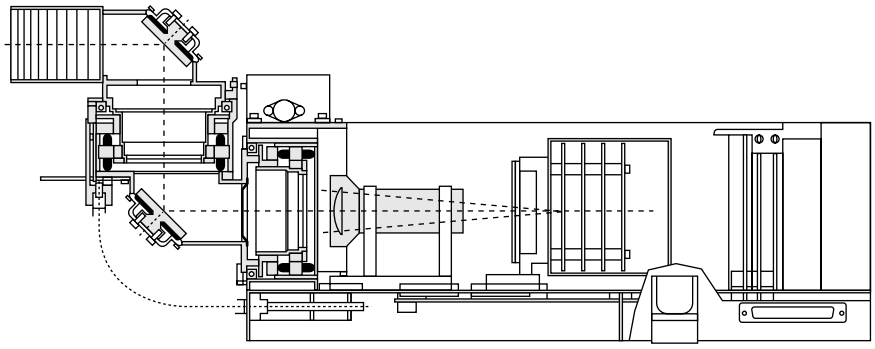

Figure 2.1: Schematic representation of a SWAN sensor unit. After Bertaux *et al.* (1995).

Since hydrogen is ionized in the vicinity of the Sun, a cavity is carved in the cloud as the Sun moves relative to it. It is precisely this interstellar hydrogen that can be seen in the SWAN maps, and the solar influence can be deduced by analyzing the topology of the cavity.

2.3.1 Instrument overview

The SWAN instrument consists of two independent but identical sensor units mounted on opposite sides of the SOHO spacecraft. Both units contain a periscope mechanism with two toroidal mirrors and local pointing accuracy of about 0.1°, which allows over 2π steradians coverage of the northern or southern ecliptic sky, respectively. The instantaneous field-of-view (FOV) of a sensor unit is 5° square divided into 5×5 pixels. The detector is of CsI cathode, multianode MCP type with MgF_2 optics, which restricts the spectral range to 115-180 nm. The original photometric sensitivity of the sensors was 0.84 counts per Rayleigh per second per pixel for the northern ecliptic unit and 0.32 for the southern one. Some degradation has taken place during the operations since launch in 1995.

Between the periscope mechanism and the detector plate is a pyrex

vessel, known as *the hydrogen absorption cell*, or H cell for short, with two MgF_2 lenses at the ends. The lenses have an equivalent focal length of 102 mm at L_α and the point spread function (PSF) of the system is about 0.3° wide at that wavelength. The chromatic aberration, however, grows rapidly towards the limits of the observing window, causing severe spreading of UV stars on the images. The vessel contains H_2 gas which can be temporarily converted to atomic hydrogen by tungsten heating filaments. An active cell removes a well-defined band around the L_α absorption line from the observed spectrum, which then gives a basic Doppler measurement capability to the instrument through comparison of normal and suppressed signals.

2.3.2 Hydrogen coma observations

The appearance of comets on SWAN maps because of the hydrogen coma produced by photodissociation of evaporated water is an additional although anticipated bonus (Bertaux *et al.*, 1995). In papers published before those included in this work, observations of comets C/1996 B2 Hyakutake (Bertaux *et al.*, 1998), 46P/Wirtanen (Bertaux *et al.*, 1999a) and C/1995 O1 Hale-Bopp (Combi *et al.*, 2000) have been discussed, and because to date well over 20 comets have been identified from the SWAN images, more publications will likely follow. The exceptionally large field of view, both instantaneous and in the sweeping mode practically limitless, ensures that the whole coma is imaged and subsequent results are thus independent of aperture-related effects. Furthermore, with the exception of the central pixel, SWAN images of cometary coma are usually well within the optically thin region which provides robust Q_{H_2O} estimates.

SWAN also provides means for removal of the background signal and compensation of short-term solar irradiation variations. The importance of the SWAN instrument in cometary studies is twofold: first, the high spatial and temporal coverage gives a definite advantage for cometary surveys as described in paper 3 of this thesis. Previously, comparable results were obtained with the Infrared Astronomical Satellite (IRAS) which detected 30 comets as a byproduct of other activities (Walker and Aumann, 1990).

Second, the remarkably stable observing conditions enable the creation of a systematic and consistent set of observations as demonstrated in paper 5 of this thesis.

2.4 Image processing

For a large part of the time during the history of astronomy, comets and other moving objects have been detected by human inspection. Slowly moving objects leave a streak to the photographic emulsion, and flipping two well aligned sky images taken some time apart back and forth makes any rapidly moving object blink noticeably. The problem with the conventional approach is that all findings are necessarily subjective. The advent of image digitizing utilities and CCD detectors has enabled automatic processing of observations and detection of minor bodies of the solar system. Operational programs based on object classification and motion detection through location matching (Rabinowitz, 1991) are used to identify potential Near-Earth Objects (NEO) for later human inspection.

A large part of the modern image processing tool set used in astronomy, including the *Richardson-Lucy Algorithm* (RLA) (Richardson, 1972; Lucy, 1974), *Maximum Entropy Method* (MEM) (Gull and Daniell, 1978) and CLEAN (Högbom, 1974), has been created to remove artifacts caused by nonzero PSF and finite aperture size but neither of these is relevant for the SWAN instrument[1]. SWAN full sky images have several very specific issues that must be taken into account when designing an automatic system for comet detection. The abundance of stars is comparable to visual observations but because of the chromatic aberration stars have the same overall shape as faint comets. Furthermore, the large background signal lowers the signal to noise ratio, the mosaic nature of sky maps in combination with poor line-of-sight (LOS) retrieval creates noise which is hard to eliminate by Wiener filtering (Andrews and Hunt, 1977). The coarse spatial resolution compared to object size makes comet detection a very challenging task.

[1]The chromatic aberration dictates that stars *do* have noticeable PSF but the small instantaneous FOV prevents effective deconvolution

An approach based on image classification is only efficient far above the noise limit and in the case of SWAN data the sensitivity threshold should be set too high for any useful purpose. Also, motion detection through object identification and position checking fares extremely poorly in the case of dense star field with large position inaccuracies. Therefore, very early during the project that led to the results presented in the first three papers of this work, it became a top priority task to design a program that is at the same time robust enough to cope with the irregularities in SWAN data, and sensitive enough to probe the region beyond the theoretical single image signal to noise limit. The optimal solution is already known: it is a probabilistic device called *Hough transform* (Ballard and Brown, 1982) but in this particular case it would be prohibitively computation intensive. To solve the problem in a more economical way it was broken into steps and a heuristic combination of partial solutions applied one after another as described in paper 2 of this thesis. The background removal is done by median difference filtering which is comparable to the better known method of enhancing fine details by overlaying the original image with an out-of-focus negative. In the digital domain this would correspond to Gaussian blurring but the median filter has a more favourable signal response close to sharp base level changes. The Laplace filter which is often used for similar purposes performs even worse with very noisy data.

The actual comet detection is distributed into three subsequent layers which can be realized as a neural network, and related terminology is used here to describe the method. The first layer fires for local temporal maxima. The reason is naturally that comets always brighten the image and thus any larger than average brightening of an image pixel may be a sign of a comet. The second layer only fires if there are enough simultaneously firing first layer nodes in the neighbourhood, with the reason that comets are extended objects and thus any single pixel maximum is likely noise. The first and second layer together create a set of possible comet detections but depending on the given firing thresholds an overwhelming majority of the signals represent spurious noise. The third layer uses a method very similar to the mentioned Hough transform to evaluate the set so as to give different combinations a probabilistic value according to how likely they represent a

trail of a comet on the sky. Even this very much reduced set would take a long time to evaluate without a proper implementation which only takes into account the most probable combinations.

The operational version of the method is fast enough by any relevant measure: a typical run on three months of data will terminate within minutes on a low-end personal computer. The results for the most part equal or even exceed human performance as verified by test trials on simulated data and the fact that one of the automatically found comets, C/1998 H1 Stonehouse (9 detections in subsequent images) could not be verified by human inspection because the comet was too faint. The ability of the method to overcome the single image noise limit is based on counting cumulative probabilities over a series of images, like combining several snapshots of one faint object taken at different times. To put things into perspective, the method described here is the fifth or seventh version in a series of progressively more successful procedures evaluated during the development phase, the exact number depending on the classifying criteria between different methods and different versions of the same method.

2.5 Size distribution

According to current understanding, comets and asteroids form the most concrete long-term threat to human existence (Chapman and Morrison, 1994) and surveys have thus recently been initiated to assess the hazards posed by large asteroids and short-period comets moving close to the ecliptic plane and regularly approaching to favourable observing range. Since their orbits can be projected far into the future, potential impacts can be predicted years in advance. These may account for 75% of the total impact hazard (Shoemaker and Wolfe, 1982; Shoemaker *et al.*, 1994). In contrast, long-period comets may approach from any direction and, because of their low albedo, they can usually be detected only inside the orbit of Jupiter when they become active, leaving preciously little time to react. On average they are also bigger and impact velocities are higher than with asteroids (McFadden *et al.*, 1989). Still even statistical impact probabilities are only

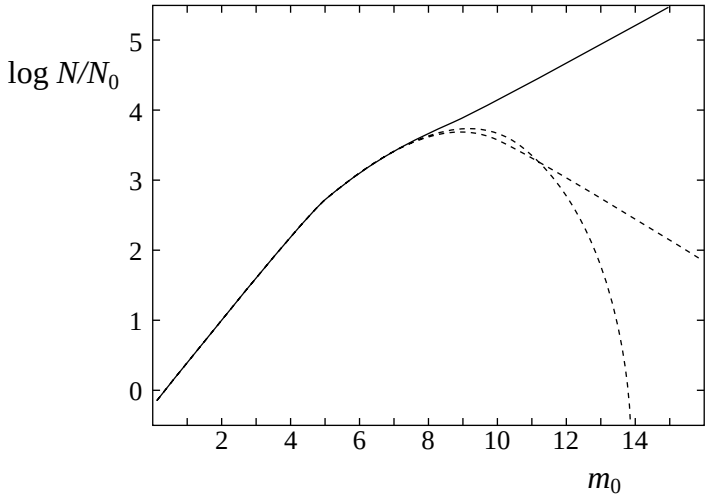

Figure 2.2: Distribution of long-period comets in arbitrary units as a function of absolute magnitude m_0. Solid line after Everhart (1967) and two alternative extrapolations suggested by Sekanina and Yeomans (1984).

tentative since to date the size distribution of comets is poorly known.

2.5.1 Small comets

Depending on the topic of discussion, "small" in the cometary context may denote anything below 1 km. The relation between the size and absolute brightness of a comet is not adequately known but often the term is used to refer to comets too faint to be observed through ordinary means. Most cometesimals of the *Kreutz sungrazer family* (Marsden, 1967, 1989) qualify in this group since they are only seen on coronagraphs, in the immediate vicinity of the Sun only moments before they are completely vaporized. Everhart (1967) tried to determine the rate at which new comets approach perihelion and found a simple power law for the cometary size distribution (Fig. 2.2). Although later studies (Kresák and Pittich, 1978; Fernándes

and Ip, 1991) suggest that he overestimated the absolute number of new comets, the power law for Earth-crossing long-period comets,

$$N(D) = N_0 \left(\frac{D}{D_0} \right)^{-1.97} \tag{2.1}$$

(Shoemaker and Wolfe, 1982) where $N_0 \approx 100/yr$ (Bowell and Muinonen, 1994) for $D_0 = 1$ km, very likely only holds for comets larger than 1 km in diameter.

A straightforward extrapolation of the Everhart distribution to smaller sizes agreed with a hypothesis based on airglow estimates suggesting that the inner solar system is continuously bombarded by large number of small cometesimals in the 1 m to 100 m range (Frank *et al.*, 1986). A validation of this hypothesis in the form of observed changes in the L_α background emission as a function of heliocentric distance was soon claimed based on Voyager 1 measurements (Donahue *et al.*, 1987) but it was later proved to be a misinterpretation (Hall and Shemansky, 1988). The use of a simple L_α instrument in detecting such small comets was suggested by Banaszkiewicz *et al.* (1989) and indeed SWAN comes close to the required performance. A clever reprogramming of the SWAN data processing path will gain a magnitude or two of sensitivity which should yield some indicative results but a conclusive answer may still lie just out of reach. Brandt *et al.* (1996a,b) have suggested the use of ultraviolet OH lines in the study of this question.

It must be noticed that small cometesimals might have a refractive mantle — a possible scenario discussed in paper 5 of this thesis as well — in which case coma-based observations would be of little use. Meteoroid observations (Ceplecha, 1994) suggest an abundant population of small bodies, and cratering records suggest that the power law holds down to about 100 m (Shoemaker *et al.*, 1982). On the other hand, Sekanina and Yeomans (1984) have noted that the number of discovered comets does not increase as expected and there may thus be far fewer small comets than predicted by others. A cutoff is suggested by Hughes (1987, 1990) and Parker *et al.* (1990) as well. The issue will remain controversial as long as direct observational evidence remains insufficient.

2.5.2 NEO surveys

Along with the discovery of the first Earth-crossing asteroids came the realization that large bodies might cause unimaginable destruction in the case of impact (Watson, 1941). The notion was not, of course, a new one but for the first time it was approached from a solid scientific background. The prospect was later sporadically mentioned by other authors as well but it did not reach public awareness until the era of space exploration around the 1980s when robotic probes sent back images of the battered terrains of various bodies of the solar system. The Spaceguard Survey report (Morrison, 1992) acknowledged the hazard and outlined plans to detect 90% of Earth-orbit crossing asteroids larger than 1 km in diameter within 25 years. Lack of funding has prevented the original concept of dedicated instruments and the work is being done on already existing facilities.

Besides the early (1973–1994) photographic *Planet-Crossing Asteroid Survey* (PCAS) (Helin and Shoemaker, 1979) at the Palomar observatory and the related *Palomar Asteroid and Comet Survey* (PACS) (1982–1996) there are several recent efforts:

- LINEAR Lincoln Laboratory Near Earth Asteroid Research project matured to operational level in 1997 and it is the most successful NEO program to date (Stokes *et al.*, 2000).

- Spacewatch Telescope of the University of Arizona (Gehrels, 1991) was the first CCD system with a semi-automated search program and it has initiated a new field of observation techniques known as "scannerscopy".

- NEAT Near-Earth Asteroid Tracking program at the Maui Space Surveillance Site is a joint effort between Jet Propulsion Laboratory (JPL) and U.S. Air Force started in December 1995.

- LONEOS Lowell Observatory Near-Earth Object Search in Flagstaff, Arizona, has been operational since 1993 (Bowell and Muinonen, 1994).

- Beijing Astronomical Observatory (BAO) Schmidt CCD Asteroid Program (SCAP) has been operational since 1996.
- Catalina Sky Survey (CSS) (Spahr *et al.*, 1996) is a continuation program with modern instrumentation for the photographic Bigelow Sky Survey (BSS) started in 1992.
- OCA-DLR Asteroid Survey (ODAS) was a joint effort between Observatoire de la Côte d'Azur, Nice, France (OCA) and Institute of Planetary Exploration, Berlin-Adlershof, Germany (DLR) from 1996 to 1999.

These surveys are optimized for detecting asteroids, although new comets regularly show up as well. The most important bias for cometary detection is the uneven coverage of the survey since observing facilities concentrate on the northern hemisphere. The discovery of the relatively bright ($\sim$ 11 mag) comet C/1997 K2 passing the southern ecliptic pole in June 1997 and only seen by the SWAN instrument as described in paper 1 of this thesis can be seen as a direct consequence of the fact that the NEO survey of the Anglo-Australian Observatory at Siding Spring, Australia (AANEAS), was terminated in 1996 because of ceased funding[2].

[2]There is an online archive for correspondence between the project coordinator, M. Paine, and various representatives of state mentioning the C/1997 K2 case at `http://www4.tpg.com.au/users/tps-seti/spacegd3.html` which illustrates well the problematic nature of funding of NEO surveys.

Chapter 3

Hydrogen coma

The basic chain of events leading to the creation of the hydrogen coma of a comet has been known for a long time. Unlike the visible dust tail, the hydrogen coma is almost spherically symmetric and an order of magnitude larger in area (Fig. 3.1). Solar irradiation vaporizes water ice from the surface of a comet, breaks it into oxygen and hydrogen atoms, excites atoms causing them to emit light at well-defined wavelengths, and finally, ionizes the atoms causing them to disappear from the SWAN images. As this simplified description points out, every step in the process depends on the solar photon flux — and to an extent on the solar wind as well. Therefore the solar output must be carefully evaluated in the context of hydrogen coma observations and $Q_{\mathrm{H_2O}}$ production rates.

3.1 Sublimation

Without dealing with details of models of cometary nucleus, a basic sublimation process is driven by solar heating of an exposed, icy surface area (Delsemme and Swings, 1952). The production rate $Z(\theta)$ as a function of the angle θ between the solar flux $F_{\odot}r^{-2}$ direction and surface normal can, neglecting the fractal nature of cometary material, be modelled with an

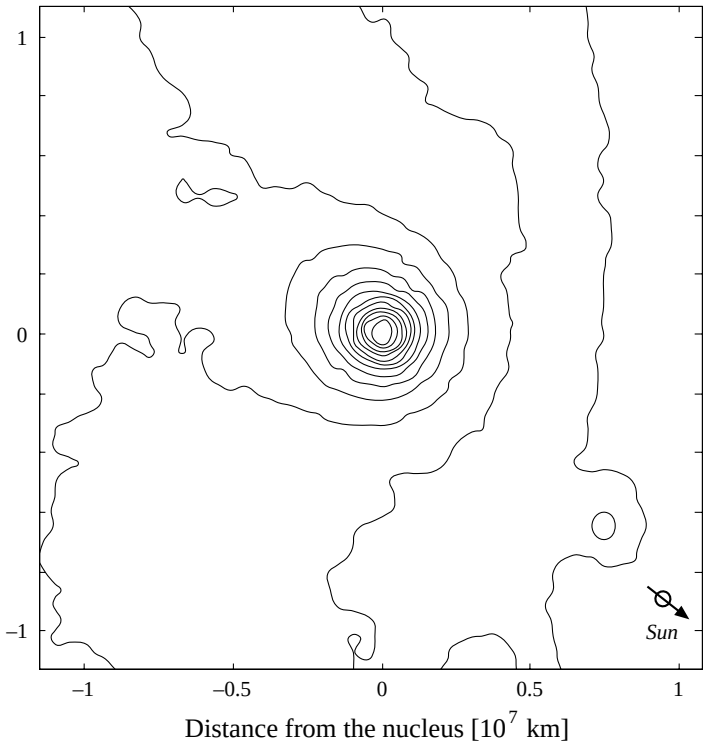

Figure 3.1: Hydrogen coma of comet D/1999 S4 LINEAR as seen by the SWAN instrument. Contours at 50 R intervals and solar direction indicated with an arrow.

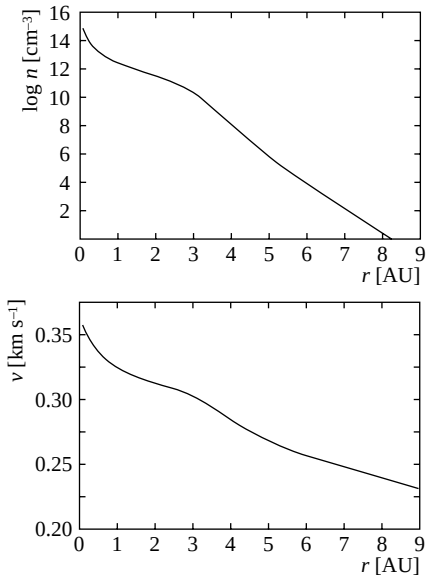

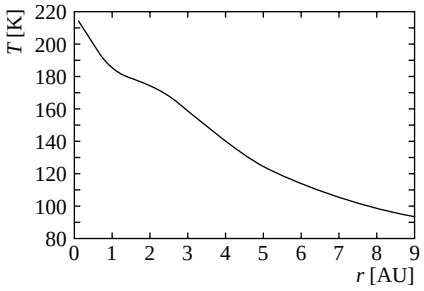

Figure 3.2: Number density, temperature and outflow velocity of evaporating gas at the surface of the nucleus for a H_2O-dominated comet as a function of heliocentric distance. After Houpis and Mendis (1981).

energy balance equation (Keller, 1990)

$$\frac{F_\odot e^{-\tau}(1-A_v)\cos\theta}{r^2} = \epsilon\sigma_0[T_\mathrm{N}(\theta)]^4 + \frac{Z(\theta)L(T_\mathrm{N})}{N_A} + \kappa\frac{dT_\mathrm{N}}{dR} \tag{3.1}$$

in conjunction with the Clausius-Clapeyron equation of state

$$p_\mathrm{N}(\theta) = p_0 \exp\left[\frac{L(T_\mathrm{N})}{kN_A}\left(\frac{1}{T_0} - \frac{1}{T_\mathrm{N}(\theta)}\right)\right] , \tag{3.2}$$

the ideal gas law

$$p_\mathrm{N}(\theta) = kn_\mathrm{N}(\theta)T_\mathrm{N}(\theta) , \tag{3.3}$$

and the escape of a gas into vacuum

$$Z(\theta) = \frac{1}{4}n_\mathrm{N}(\theta)\left[\frac{kT_\mathrm{N}(\theta)}{2\pi m}\right]^{1/2} \tag{3.4}$$

where τ is the optical depth of the coma, A_v the Bond albedo, ϵ the surface IR emissivity, κ thermal conductivity, L the latent heat of sublimation,

$T_N(\theta)$ the surface temperature, R the nuclear radius, $p_N(\theta)$, $n_N(\theta)$ and m the pressure, number density and specific molecular mass of the gas, p_0 and T_0 the pressure and temperature at some reference point, and σ_0, k and N_A the Stefan-Boltzmann and Boltzmann constants and the Avogadro number, respectively. The behaviour of an H_2O-dominated flow is depicted in Fig. 3.2. Early applications of this model (Delsemme and Rud, 1973) led, however, to unrealistically high estimates of surface albedo, which could later in the light of Halley observations be explained by the fact that cometary activity can be constrained to small regions of the surface. Also, if the process is dominated by subsurface sublimation, the escaping gas may be heated by the mantle which is close to the black body temperature and thus the temperature and escape velocity of H_2O can differ from the presented values.

3.1.1 Extended emission

It was realized a long time ago that the surface of the nucleus may not be the only source of cometary emission. The dust entrained by the gas flow may have an icy mantle which subsequently vaporizes, creating an extended area of emission around the nucleus. The existence of a micrometer-sized grain halo around the nucleus was first suggested by Huebner and Weigert (1966) but the fast sublimation rate of particles implies that such a halo cannot extend far from the surface. Based on laboratory experiments (Delsemme and Wenger, 1970) of sublimation of clathrates, Delsemme and Miller (1970, 1971) suggested the existence of larger, submillimeter to millimeter-sized grains of ice released into the gas flow to explain the observed features of C/1959 Y1 Burnham, and A'Hearn *et al.* (1984) suggested that an outburst in comet C/1980 E1 Bowell at 4.5 AU produced a large number of such particles, causing the observed peak in OH production. Still even grains in this size range will under normal circumstances dissipate completely within the inner coma where the flow is hydrodynamic. There is one related process which does not, however, contribute to the total emission: Yamamoto and Ashihara (1985) have demonstrated that the rapid cooling of gas as it expands into vacuum can lead to temporary recondensation of icy particles.

This process is only important for energy balance considerations and possibly to coma chemistry.

Mäkinen *et al.* (paper 5 of this thesis) suggested, based on the apparent discrepancy between Q_{H_2O} and the total mass of dissipated water, that the observed Q_{H_2O} of comet C/1999 S4 LINEAR was largely driven by the sublimation of fragmentation-related particles. Also, hydrogen emission in the 10^7 km range away from the nucleus has been detected from the SWAN observations of C/1995 O1 Hale-Bopp by Mäkinen (manuscript to be submitted in 2001) as described in the concluding Chapter of this thesis.

3.1.2 Fragmentation

Although comets in general appear to be consolidated bodies, many of them seem to have extremely low cohesion as demonstrated by frequent observations of splitting, fragmentation and decay of both short- and long-period comets (Sekanina, 1982, 1997). Ripped apart by tidal forces, rotation, sublimation of icy glue between structural units or explosive release of subsurface pockets of volatiles, comets may split in two like 3D/Biela, or into more numerous fragments: the comet C/1975 V1 West broke into four major fragments and the famous D/1993 F2 Shoemaker-Levy 9 was broken into 21 major pieces by a close encounter with Jupiter (Sekanina *et al.*, 1994). Fragmentation events close to the perihelion passage may disrupt the nucleus completely as was witnessed in the recent case of C/1999 S4 LINEAR, which seems to belong to a special class of dissipating comets (Sekanina, 1984), or if the parent nucleus is big enough, fragmentation can result in a whole new population of comets on almost parallel orbits, like the Kreutz sungrazer family. A total of 15 small sungrazers was detected from SOLWIND (Sheeley *et al.*, 1982) and *Solar Maximum Mission* (SMM) coronagraphs (MacQueen and St. Cyr, 1991) but their abundance has only recently been realized from *Large Angle and Spectrometric Coronagraph Experiment* (LASCO/SOHO) coronagraphs (Biesecker *et al.*, 1999).

In the course of preparing paper 5 of this thesis, it became necessary to model the dissipation process of cometary fragments. Because the presentation there had to be concise, details of the model were left out. They

are discussed here for the sake of completeness. If at first a homogeneous sphere of radius R composed mainly of water ice is heated by solar irradiation, then the water production rate $q(t)$ can be expressed as

$$q(t) = \pi W R^2(t) \tag{3.5}$$

where

$$W(r) = \frac{F_\odot N_A (1 - A_v)}{L r^2} \tag{3.6}$$

represents sublimation per unit area as a function of heliocentric distance r. Compared to Eq. 3.1, various terms like optical thickness and conductivity have been omitted, because the minimal surface is being estimated, and these terms would only increase the surface. The mass loss of the sphere is obtained from Eq. 3.5

$$\frac{dm}{dt} = -18uq(t) \tag{3.7}$$

where $u = 1.67 \times 10^{-27}$ kg is the atomic mass unit. Assuming density ρ the change in volume of the sphere is thus

$$\frac{dV}{dt} = -\frac{18uq(t)}{\rho} = 4\pi R^2 \frac{dR}{dt} \tag{3.8}$$

Differentiating Eq. 3.5 and substituting Eq. 3.8 yields an equation for $q(t)$ if the change in $W = W(r(t))$ is small compared to $d_t R$

$$\frac{dq}{dt} = 2\pi W R \frac{dR}{dt} = -\frac{9u\pi^{1/2} W^{3/2}}{\rho} [q(t)]^{\frac{1}{2}} \tag{3.9}$$

The water production rate of N identical spheres is thus

$$Q(t) = Nq(t) = \pi W N R^2(t) \tag{3.10}$$

and hence

$$\frac{dQ}{dt} = -\frac{9u(\pi N)^{1/2} W^{3/2}}{\rho} [Q(t)]^{\frac{1}{2}} \tag{3.11}$$

The behaviour of this model was compared to the observed dissipation curve of C/1999 S4 and found to be insufficient to yield even a rudimentary agreement.

Developing the model further, an ensemble of spheres of different sizes can be simulated. A reasonable approximation is to consider m groups of spheres with the number of spheres in group i given by

$$N_i = N_0 b^i,\ i = 0, \ldots, m-1 \tag{3.12}$$

where b defines intergroup multiplier. Of the two parameters m must have an integer value but b can be varied continuously. Although fractional values for the number of spheres in a group are not logically meaningful, they make sense from the physical point of view since it compensates for the approximation of a coarse model which assumes that within each group all spheres are of the same size, their radii given by the equation

$$R = fN(R)^{-1/\alpha} \tag{3.13}$$

where α is some positive number and the constant f can be solved as

$$f = \left(\frac{Q}{\pi W \sum_i N_i^{1-2/\alpha}} \right)^{\frac{1}{2}} \tag{3.14}$$

Then the total $Q_{\mathrm{H_2O}}$ can be presented as a sum of partial water production rates of each group

$$Q = \sum_i Q_i \tag{3.15}$$

where the initial partial rates become

$$Q_{i0} = Q_0 \frac{N_i R_i^2}{\sum_i N_i R_i^2} = Q_0 \frac{N_i^{1-2/\alpha}}{\sum_i N_i^{1-2/\alpha}} \tag{3.16}$$

In the operative equation (3.11) the bulk density needs to be given. A sensible approach is to give it as a function of the initial mass of water M_0

$$V = \frac{4\pi}{3} f^3 \sum_i N_i^{1-3/\alpha} = \frac{M_0}{\rho} \tag{3.17}$$

$$\rho = \frac{3M_0}{4\pi f^3 \sum_i N_i^{1-3/\alpha}} \tag{3.18}$$

Although in principle the mass can be calculated *a posteriori* from

$$M_0 = 18u \int_0^\infty dt Q(t) \tag{3.19}$$

the most straightforward approach, applied in paper 5, is to fix m and N_0 by hand and then fit the model to observed values with b, α and M_0 as free parameters. It must be stressed that because of the order in which the quantities are calculated, N_0 does not change the solution itself, only the bulk density. Therefore, once a solution has been found, N_0 and ρ can be determined if either of them is known. Another point worth mentioning is the fact that the important results obtained through the optimization process, α and M_0, are (provided that the size distribution is relatively continuous) fairly independent of the actual nature of fragments, be they homogeneous, differentiated or fractal in composition, or spherical, flat or even needle-like in shape.

3.1.3 Collision zone

The evaporating gas forms a neutral coma in which two physically different regions can be observed: the relatively dense inner coma also called the *collision zone*, and the collisionless exosphere. Assuming representative values for number density n and an H_2O molecular cross-section of $\sigma = 10^{-19}$ m^2, the molecular mean free path

$$\Lambda = \frac{1}{\sqrt{2} n \sigma} \tag{3.20}$$

just above the surface of the nucleus is typically of the order of one meter which is small enough for the flow to be described with the hydrodynamic model. The one-component equations can be written as

$$\begin{gathered} \frac{\partial \rho}{\partial t} + \nabla \cdot (\rho \mathbf{v}) = \dot{\rho} \\ \frac{\partial}{\partial t}(\rho \mathbf{v}) + (\mathbf{v} \cdot \nabla)\rho \mathbf{v} + \rho \mathbf{v}(\nabla \cdot \mathbf{v}) + \nabla p = \dot{\mathbf{p}} \\ \frac{\partial}{\partial t}\left(\tfrac{1}{2}\rho v^2 + \rho e\right) + \nabla \cdot \left[\rho \mathbf{v}\left(\tfrac{v^2}{2} + h\right)\right] = \dot{E} \end{gathered} \tag{3.21}$$

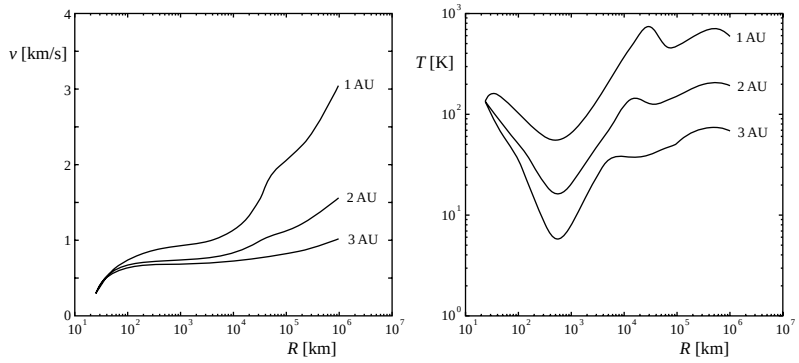

Figure 3.3: Simulated outflow velocity and kinetic temperature of gas as a function of distance from the center of the nucleus of C/1995 O1 Hale-Bopp. After Combi *et al.* (1997).

(Schmidt *et al.*, 1988) where e and h are the internal specific energy and enthalpy, and the right hand terms represent sources and sinks of mass, momentum and energy, respectively. When several species are considered, the above set of equations is separately applied to each species and the right hand terms then contain coupling coefficients between species. Typical behaviour of the velocity and temperature of the expanding gas is depicted in Fig. 3.3.

3.1.4 Exosphere

As the gas expands to vacuum the hydrodynamic approximation soon breaks up and the exosphere is dominated by photolytic processes. The boundary between the two different domains cannot be described analytically, which has made Monte Carlo methods the conventional approach, although the collision zone can also be treated as a secondary source of emission which emits particles into the exosphere (Huebner and Keady, 1984). The exact boundary between the inner atmosphere and exosphere is arbitrary but it is conventionally set to the distance where a particle has a

probability 0.5 of escaping to infinity without further collisions which leads to a typical size of the order of 10^4 km for the radius R_c of the collision sphere. The molecules and atoms feel the solar radiation pressure caused by the fact that the impulse vectors of absorbed solar photons all point in the same direction but those of emitted photons are randomly distributed, which leads to accumulation of excess impulse. The effective acceleration is

$$a = \frac{h}{mr^2} \sum_i \frac{g_i}{\lambda_i} \tag{3.22}$$

where h is the Planck constant, m particle mass, r heliocentric distance in AU, g_i the fluorescent emission rate or g-factor for transition i, and λ_i the corresponding wavelength. For atomic hydrogen the L_α resonance dominates and a is in the 10^{-3} m s^{-2} range which over the lifetime of H I corresponds to a net displacement of about 10^6 km.

3.2 Photolysis

The two most important photolytic processes are photodissociation and photoionization. In the case of water emission, the former is responsible for breaking H_2O to OH and H and to a lesser extent to O and H_2 (Crovisier, 1989), and the latter ionizes neutral hydrogen atoms to produce protons. There are several complications to this basic picture: there is a contribution from parent molecules other than H_2O, some parent molecules are ionized right away, some daughter molecules are created directly in an excited state, solar wind particles account for a small number of processes and the dissociation rates for different channels and thus total branching ratios depend on the variable solar irradiation.

3.2.1 Solar flux

The solar activity varies over many different time scales. For the purpose of cometary studies the most important periods are the (average) 27-day solar rotation period and the 11-year solar cycle whose low and high activity periods are referred to as the quiet and active Sun, respectively. The

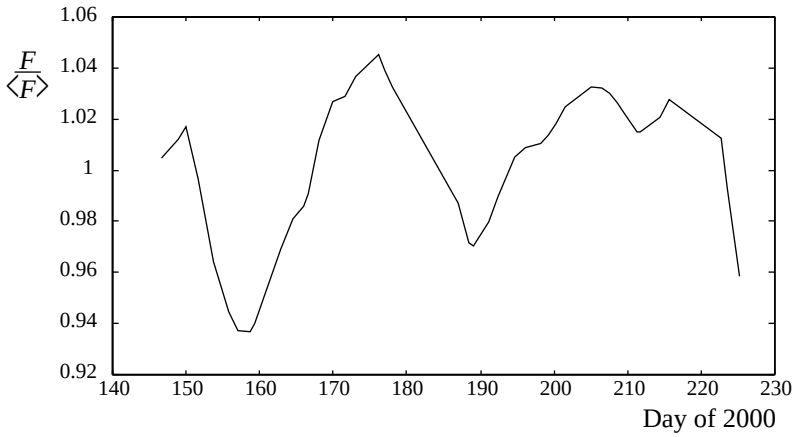

Figure 3.4: Relative variations in solar L_α irradiation for C/1999 S4 LINEAR derived from background H I emission observations of the SWAN instrument.

total intensity variations between the extremes depend on the wavelength. For the L_α line there is a factor of two difference in the average intensity (Buzdien *et al.*, 1994). The conventional approach of listing the relevant parameters for active and quiet Sun conditions, respectively, has the intrinsic shortcoming of a poorly defined input parameter, since solar cycles are not identical. A more unambiguous way is to correlate the photolysis rates to known indicators of solar activity, as has recently been done by, e.g., Buzdien *et al.* (1994) and Wegmann *et al.* (1999). Frequently used indicators are the 10.7 cm radio flux and the He I 1083 nm equivalent width, and direct observations of L_α by various satellite instruments.

Although not designed for the purpose, the SWAN instrument can be used to estimate variations in the local L_α irradiation field as well. This has so far been used twice, for C/1997 K2 (paper 1) and C/1999 S4 LINEAR (paper 5) because both comets featured characteristics that required rigorous estimation of L_α variations. As will be discussed in the last Chapter, the

SWAN instrument has almost 4π sr coverage of the sky and thus observed variations in the background intensity can be deconvolved to obtain the variations at the source. At the moment, however, the complete solution is beyond available resources, and a good approximation is achieved by monitoring intensity variations at different patches of background sky located along the trail of the comet in question. Measurements a sufficient distance on either side are required so that the passing comet does not affect them. The relative variations are then interpolated for the exact location of the comet, taking into account solar rotation period. The obtained variation profile for C/1999 S4 is depicted in Fig. 3.4. This method is still quite rudimentary and requires further study but in principle it is superior to the usual proxy methods for two reasons: the observed quantity is exactly the resonant L_α fluorescence without the need to incorporate any model parameters, and second, the virtually full coverage of the radiation field has vastly better angular resolution than any experiment which integrates over the visible solar hemisphere. The difference would become especially pronounced for comets far away from the ecliptic plane.

3.2.2 Dissociation

Starting with the photodissociation of water, the channels and their respective rates are given in Table 3.1. The branching ratios for the channel $98 < \lambda < 145$ nm are poorly known but since the total rate of this channel is small, the ratios are regularly assumed to be of the same order as in the L_α channel. In addition to this, there are several channels for different ion-neutral interactions between the coma and solar wind as discussed in Buzdien *et al.* (1994) and Wegmann *et al.* (1999) but these have small dissociation rates compared to photolysis. The produced H and OH have excess velocities of 20 $\mathrm{km\,s^{-1}}$ and 1 $\mathrm{km\,s^{-1}}$ relative to their center of mass. Produced H_2 has a relatively long lifetime of $\tau = 6 \times 10^6$ s (Huebner *et al.*, 1992) and dissociated H atoms receive large excess velocities. Therefore H_2 has negligible contribution to column densities.

Photodissociation of the hydroxyl radical is more complicated. Dissociation rates for major channels and resulting products are given in Ta-

Table 3.1: Photodissociation of water. Rates for 1 AU are given for quiet σ_q and active σ_a Sun. The values are based on Buzdien *et al.* (1994) and Wegmann *et al.* (1999).

Channel	σ_q [10^{-6} s^{-1}]	σ_a [10^{-6} s^{-1}]	Products	
$\lambda > 145$ nm	4.91	5.42	99%	$H + OH(X^2\Pi)$
			1%	$O + H_2$
$\lambda = 121.6$ nm	4.32	6.48	70%	$H + OH(X^2\Pi)$
			8%	$H + OH(A^2\Sigma^+)$
			10%	$O(^1D) + H_2(X^1\Sigma_g^+)$
			12%	$O(^3P) + 2\,H$
$98 < \lambda < 145$ nm, $\lambda \neq 121.6$ nm	0.68	1.09	assume L_α values	
$\lambda < 98$ nm	0.52	1.16	86%	$H_2O^+ + e^-$
			14%	$OH^+ + H + e^-$

ble 3.2 with tabulated end product velocities. In addition to this, the $A^2\Sigma^+(v' = 2, 3)$ channel with σ in the range of 2.49–5.41 $\times\, 10^{-6}$ s^{-1} (Van Dishoeck and Dalgarno, 1984) depends very much on the heliocentric velocity and the related lifetime is depicted in Fig. 3.5. The corresponding velocities are $v_H = 8$ km s^{-1}, $v_O = 0.5$ km s^{-1} for $v' = 2$ and $v_H = 11$ km s^{-1}, $v_O = 0.5$ km s^{-1} for $v' = 3$ (Van Dishoeck and Dalgarno, 1984). As with water dissociation, the hydroxyl dissociation rates for solar wind interaction are small compared to photolysis (Wegmann *et al.*, 1999).

Photodestruction of H atoms differs from the previous processes because it is caused primarily by solar wind interaction rather than photolysis. Charge exchange with solar wind protons is the dominant process and although it does not change the number density of H I atoms, the created neutral atom usually has a sufficiently large Doppler shift to make it invisible for L_α fluorescence. Electron impact and photoionization are the

Table 3.2: Photodissociation of OH. Rates for 1 AU are given for quiet σ_q and active σ_a Sun and end product velocities are tabulated for each channel. The values are based on Buzdien *et al.* (1994) and Van Dishoeck and Dalgarno (1984).

Channel	σ_q	σ_a	Product	v_H	v_O
	$[10^{-6}s^{-1}]$			$km\,s^{-1}$	
$1^2\Sigma^-$	1.40	1.58	$O(^3P) + H$	22–26	1.6
$1^2\Delta$	0.38	0.57	$O(^1D) + H$	26.3	1.6
$2^2\Pi$–$3^2\Pi$	0.24	0.39	$O(^1D) + H$	26.3	1.6
$B^2\Sigma^+$	0.05	0.08	$O(^1S) + H$	17.1	1.1
ionization	0.25	0.47	$OH^+ + e^-$		

two destructive processes. This leads to highly variable hydrogen lifetimes (Combi *et al.*, 1986) which depend on local solar wind velocity, density and temperature. Since the solar wind parameters have local variations which cannot be observed remotely, in addition to a latitudinal anisotropy (Bertaux *et al.*, 1999b), several approaches to determining the hydrogen lifetime have been suggested. Either, one can use some average value suitable for the current phase of the solar cycle (Keller and Meier, 1976), or a value based on observed solar wind and UV fluxes (Combi *et al.*, 1986), or leave hydrogen lifetime as a free parameter to be solved by comparison of a coma model with observations.

3.2.3 Coma density model

Combining the data in previous Sections, the basic monokinetic model of the H I exosphere was presented by Haser (1957). For the simplest reaction tree $H_2O + h\nu \rightarrow OH + H^1$, $OH + h\nu \rightarrow O + H^2$ the radial number density

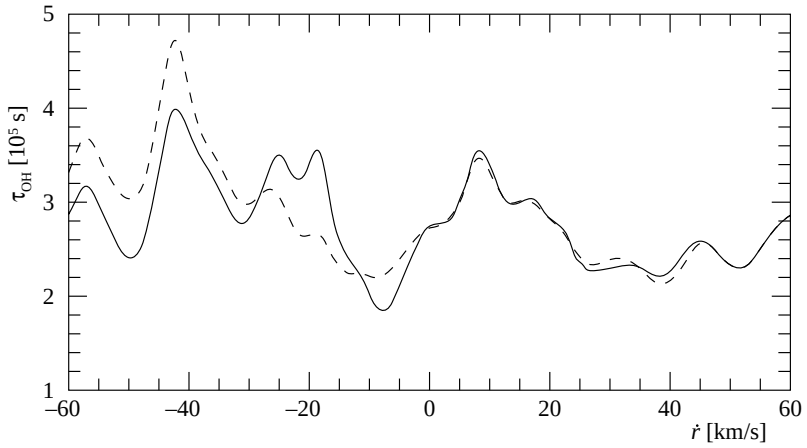

Figure 3.5: Predissociation lifetime of OH from the $A^2\Sigma^+$ state at 1 AU as a function of heliocentric velocity $\dot{r}$ for unquenched (solid line) and quenched (dashed line) inversion. After Schleicher and A'Hearn (1988).

of the first hydrogen population becomes (Festou, 1981)

$$n_{\mathrm{H}^1}(R) = \frac{Q_{\mathrm{H_2O}}}{4\pi R^2 v_{\mathrm{H}^1}} \frac{\gamma_{\mathrm{H_2O}}}{\gamma_{\mathrm{H}^1} - \gamma_{\mathrm{H_2O}}} \left[e^{-\gamma_{\mathrm{H_2O}} R} - e^{-\gamma_{\mathrm{H}^1} R} \right] \tag{3.23}$$

where $\gamma_i = 1/\Lambda_i = \sigma_i / v_i$ are the inverse scale lengths of respective species, and the number density of the second population becomes

$$n_{\mathrm{H}^2}(R) = \frac{Q_{\mathrm{H_2O}}}{4\pi R^2 v_{\mathrm{H}^2}} \left[A e^{-\gamma_{\mathrm{H_2O}} R} + B e^{-\gamma_{\mathrm{H}^2} R} + C e^{-\gamma_{\mathrm{OH}} R} \right] \tag{3.24}$$

where the coefficients A, B and C are defined as

$$\begin{aligned} A = &\ \frac{\gamma_{\mathrm{H_2O}}}{\gamma_{\mathrm{H}^2} - \gamma_{\mathrm{H_2O}}} \left(1 + \frac{\gamma_{\mathrm{H_2O}}}{\gamma_{\mathrm{OH}} - \gamma_{\mathrm{H_2O}}} \right) \\ B = &\ -A + \frac{\gamma_{\mathrm{H_2O}} \gamma_{\mathrm{OH}}}{(\gamma_{\mathrm{OH}} - \gamma_{\mathrm{H_2O}})(\gamma_{\mathrm{H}^2} - \gamma_{\mathrm{OH}})} \\ C = &\ -(A + B) \end{aligned} \tag{3.25}$$

Correspondingly, the column densities for the two populations become

$$N_{\mathrm{H}^1}(p) = \frac{Q_{\mathrm{H_2O}}}{4\pi R^2 v_{\mathrm{H}^1}} \frac{\gamma_{\mathrm{H_2O}}}{\gamma_{\mathrm{H}^1} - \gamma_{\mathrm{H_2O}}} \left[f(\gamma_{\mathrm{H_2O}} p) - f(\gamma_{\mathrm{H}^1} p) \right] \tag{3.26}$$

and

$$N_{\mathrm{H}^2}(p) = \frac{Q_{\mathrm{H_2O}}}{4\pi R^2 v_{\mathrm{H}^2}} \left[A f(\gamma_{\mathrm{H_2O}} p) + B f(\gamma_{\mathrm{H}^2} p) + C f(\gamma_{\mathrm{OH}} p) \right] \tag{3.27}$$

where p is the projected distance of the column from nucleus and the function f can be expressed as

$$f(x) = 2 \int_0^{\pi/2} d\alpha \, \exp\left(-\frac{x}{\cos\alpha} \right) \tag{3.28}$$

where the angle α denotes integration along the column.

The model described above does not take into account solar radiation pressure and the fact that the velocity vectors of dissociation products are isotropically distributed (Dolginov and Gnedin, 1966) instead of pointing radially outwards from the nucleus as assumed. A vector model was presented by Festou (1981) to overcome this shortcoming but a good approximation for the vector model can also be obtained with a Haser model using fictitious scale lengths Λ' which are related to the physical ones as (Combi and Delsemme, 1980)

$$\begin{aligned} (\Lambda'_d)^2 - (\Lambda'_p)^2 &= (\Lambda_d)^2 - (\Lambda_p)^2 \\ \frac{\Lambda'_p}{\Lambda'_d} &= \frac{\Lambda_d v_p + \Lambda_p \sqrt{v_p^2 + v_e^2}}{\Lambda_p v_p + \Lambda_d \sqrt{v_p^2 + v_e^2}} \frac{\Lambda_p}{\Lambda_d} \end{aligned} \tag{3.29}$$

where the subindices p and d denote parent and daughter species, respectively, and v_e is the average daughter velocity perpendicular to parent velocity. This modified model can be used to estimate the total water production rate of a comet for wide aperture observations even if it does not recreate observed isophote contours. The approximation of two hydrogen atom populations with very narrow velocity distributions is a reasonable one for small comets where most hydrogen atoms are produced outside the collision zone. In large comets like C/1995 O1 Hale-Bopp, however, collisional thermalization of hydrogen atoms is an important process (Fig. 3.6).

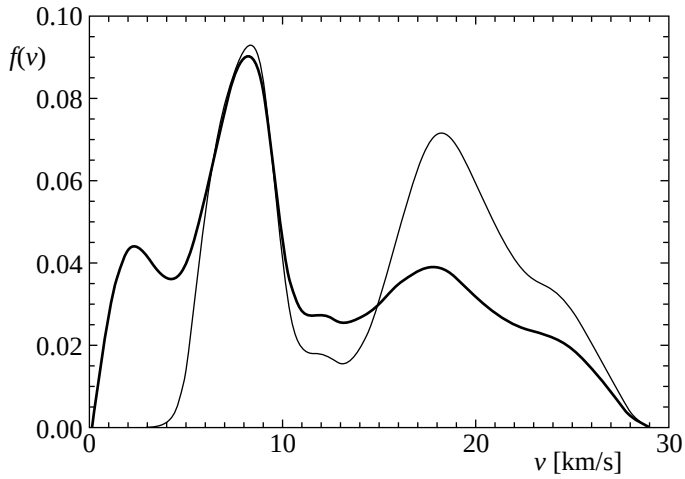

Figure 3.6: Simulated speed distribution of hydrogen atoms exiting the collision zone of C/1995 O1 Hale-Bopp at perihelion with (thick line) and without (thin line) collisional thermalization. After Combi *et al.* (2000).

3.3 Fluorescence

The process of excitation of a molecule or atom by a solar photon and the subsequent decay in one or several steps, emitting photons at wavelengths characteristic for the species, is called fluorescence, and it is the primary mechanism through which information on composition of cometary coma is obtained with spectroscopy. The emission is characterized by the g-factor which for a simple case where multiple excitations can be neglected can be expressed as

$$g = \rho_{ik} B_{ik} \frac{A_{kj}}{\sum_{j<k} A_{kj}} \tag{3.30}$$

where B_{ik} and A_{kj} are the Einstein coefficients for absorption and emission, and ρ_{ik} is the density of solar radiation at absorption frequency ν_{ik} at 1 AU. For neutral hydrogen with resonant L_α fluorescence the only relevant

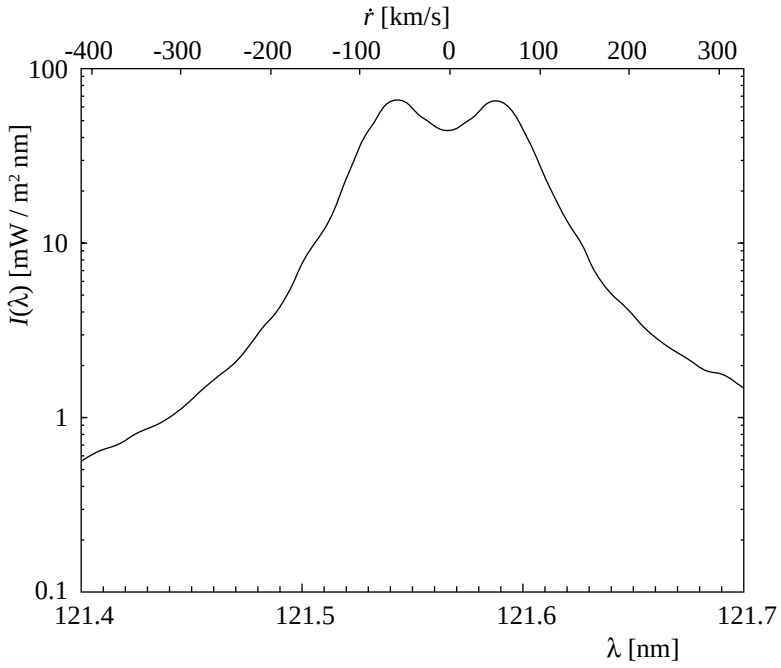

Figure 3.7: Solar irradiation profile around the Lyman α line at 121.6 nm with corresponding heliocentric velocity of the comet affecting the g-factor. After Lemaire *et al.* (1998).

mechanism, it can be written as

$$g_0 = \frac{\pi e^2}{m_\mathrm{e} c} f_\alpha F_\odot \tag{3.31}$$

(Oxenius, 1965) where e and m_e are the electron charge and mass, respectively, $f_\alpha = 0.416$ the L_α oscillator strength and $F_\odot$ the solar flux.

The velocity of a hydrogen atom relative to the Sun causes a Doppler shift to the solar spectrum and the effective flux density for the absorption band changes accordingly. The Doppler shift caused by the heliocentric ve-

locity of a comet was first considered by Swings (1941) although the term "Swings effect" usually refers to changes caused by the very complex profile of the solar spectrum above ~ 140 nm. The solar L_α profile depicted in Fig. 3.7 is very regular and the $\dot{r}$-dependence of the neutral hydrogen g-factor can be determined with good confidence. In addition to the heliocentric velocity of the comet hydrogen atoms also have some velocity relative to the nucleus and this component causes the "Greenstein effect" (Greenstein, 1958). Based on g-factors, the brightness of a column of gas can be expressed as

$$B = 10^{-6} g_0 \frac{N_\mathrm{H}}{r^2} \tag{3.32}$$

where B is the surface brightness in Rayleigh (10^{10} photons per $(4\pi)\,\mathrm{sr\,m^2\,s}$), or taking into account the Doppler effect

$$B = \frac{10^{-6}}{r^2} \int ds\, g_{\dot{\mathbf{R}}(s)} n_\mathrm{H}(\mathbf{R}(s)) \tag{3.33}$$

with integration along the line of sight.

3.3.1 Multiple scattering

The optical thickness of a hydrogen coma is

$$\tau_\mathrm{H} = \frac{\pi e^2}{m_\mathrm{e} c} f_\alpha \frac{1}{\sqrt{\pi}\Delta_\alpha} \mathrm{N_H} \tag{3.34}$$

where Δ_α is the width of the emission line which can be expressed as

$$\Delta_\alpha = \frac{\nu_0}{c} \sqrt{\frac{2kT}{m_\mathrm{H}}} \tag{3.35}$$

where ν_0 is the base frequency, k the Boltzmann constant, T the apparent temperature and m_H the mass of hydrogen atom. With numerical values the relation becomes

$$\tau_\mathrm{H} = \frac{5.9 \times 10^{-12}}{\sqrt{T}} \mathrm{N_H} \tag{3.36}$$

(Bertaux *et al.*, 1998) and using a representative temperature of $T = 5 \times 10^3$ K (Drake *et al.*, 1976) it can be noticed that the optically thin model is almost always valid for SWAN observations save perhaps the central pixel. Multiple scattering models like that by Keller (1973) are only required in reproducing the intensity profile for the innermost coma, and even then a more robust $Q_{\mathrm{H_2O}}$ estimate can be obtained by observing the optically thin region.

Chapter 4

Future prospects

Cometary studies have acquired undeniable impetus for the foreseeable future because of the interdisciplinary importance of comets and because many unanswered questions will remain even after the currently deployed or prepared cometary missions. This last Chapter discusses various research initiatives related to SWAN studies and documents ongoing or foreseen activities that are needed to manage the mission successfully.

4.1 Space missions

In the recent years several cometary missions have been initiated which, in the long run, will provide definite answers to many important questions. If various types of missions are considered in the order of relative difficulty to realize, then the first rung of the ladder, a flyby mission of a short-period comet, has already been climbed. The next steps will contain rendezvous and orbiting, then landing on the surface and ultimately, return of samples back to Earth. All of these missions will, of course, be directed to short-period comets whose orbits can be predicted years in advance. Catching a long-period comet with the current propulsion technology would require unfeasibly long storage of satellites on very eccentric parking orbits around the Earth in anticipation of an improbable chance event, appearance of a

new comet with suitable orbital parameters. This kind of a mission might, however, become possible by the same kind of recycling of a venerated satellite that happened with ISEE-3, if at some future occasion heavenly bodies happen to align themselves favourably.

There are several comet-related space missions underway which belong to different stages of exploration as described above:

Deep Space 1 After some initial difficulties, this experimental technology platform is currently on its way to encounter comet 19P/Borrelly near perihelion in September 2001.

Stardust Launched in February 1999, the spacecraft will encounter comet 81P/Wild 2 in January 2004, collect dust grains and volatiles from the coma and return the samples back to Earth in 2006.

CONTOUR The Comet Nucleus Tour spacecraft featuring a mass spectrometer, dust analyzer and an imaging spectrograph will fly by three comets during its six-year mission: 2P/Encke in November 2003, 73P/Schwassmann-Wachmann 3 in June 2006 and 6P/d'Arrest in August 2008.

Deep Impact The spacecraft will encounter comet 9P/Tempel 1 in July 2005 and deliver a 500 kg projectile which will excavate pristine subsurface material. The resulting plume of debris will also be remotely observable.

Rosetta To be launched in January 2003, Rosetta will become the first spacecraft orbiting a comet after its rendezvous with 46P/Wirtanen in November 2011. It will also deliver a probe which will land on the surface of the nucleus.

CNSR in the NASA Strategic Plan 2000 (`http://www.plans.nasa.gov/`) the Comet Nucleus Sample Return mission is scheduled for a comparable time frame as Rosetta but cruise times are to be significantly reduced by the use of ion propulsion technology.

Paper 4 of this thesis deals with the aspect of observing the target body of the mission in advance to provide necessary information for mission planning. Another important contribution comes from remote observations conducted during spacecraft operations to complement *in situ* measurements.

4.2 SWAN and beyond

The nominal end of mission for the SOHO spacecraft was in 1999 but the mission has already been extended to the end of April 2002. By then the SWAN instrument will have recorded close to 600 full sky maps and yielded observations of over 30 comets and many other objects as well. Even the basic processing and publication of these data is a large task that will keep dedicated researchers occupied well past the shutdown of the instrument. To date, over one half of comet related papers that use SWAN data are presented in this thesis and the amount will likely triple or even quadruple in the course of SWAN related cometary studies. Even a further extension of SOHO operations is not impossible, provided that the instruments keep on yielding valuable new observations.

The net importance of SWAN cometary observations lies in the large number of consistent observations which, like the spectra taken by IUE, provide means for comparison of different comets as well as monitoring the behaviour of individual comets usually through the entire apparition. After SWAN has been decommissioned, there will not be any comparable wide FOV facility flying in space for some time. There remains, however, a need for continuous SWAN-style monitoring of the sky for solar activity and comets alike, and it would be most desirable to retain this functionality in the future by some "SuperSWAN" with comparable FOV but higher spatial resolution and a more varied filtering scheme, possibly of wheel type, including a BaF_2 filter[1] to compensate finally for the troublesome stellar background signal. It would also be extremely useful if observations could

[1]Such a filter is already glued on top of one additional sensor pixel on the side of the central 25 pixels in the northern ecliptic unit but it has not been utilized so far. Besides, the most problematic area of star contamination lies on the *southern* hemisphere.

be conducted at the 308.5 nm OH 0–0 transition as well. Small-aperture instruments with these capabilities are already available and their number is probably increasing in the future, but despite their higher resolution it is not feasible to conduct systematic sky surveys with such instruments because frequent and complete coverage of the whole sky is more important.

4.2.1 New observations

The types of observations used in this work — full sky and comet-specific maps — are only some of the possibilities provided by the instrument. In the future many other kinds of observations can be made, and the data from currently unused observations can be processed to give new information. Such fields of study include:

Hydrogen cell observations Incoming light goes through a chamber containing hydrogen gas. This gas can be changed to monoatomic hydrogen by applying a current in the heater coil. This way, a sharp notch can be made to the spectrum at the L_α line and the comparison of normal to filtered signal gives a coarse doppler measurement for the velocity of fluorescing gas. This has obvious uses in cometary coma observations.

Geocorona The geocorona was easiest to observe at the beginning of the mission when the spacecraft had not yet reached its nominal position. The Earth is occassionally occulted by the spacecraft and always stays close to the anti-sunward data gap but good results could be achieved through the use of these data.

Leonids Besides observing the parent body of the Leonid shower, the comet 55P/Tempel-Tuttle, SWAN can be used to observe the trail itself by two different methods: observing the geocorona to detect any excess hydrogen possibly released by impacting debris, and directly observing the radiant or anti-radiant point so that the integrated column density along the trail could exceed detectable limits. These observations have been made but not yet analyzed and the

predicted major storm for November 2001 Leonids might give even better chances of success.

Solar system bodies Other planets, most likely Venus and Mars, could be observed. The Moon is of sub-pixel size and should appear darker than the background in the images but during a meteor shower a transient hydrogen plume might be observable on the southern pole if enough water is vaporized by impacts. All these observations require long signal integration times like cometary observations far away from the perihelion.

Stars Known occultations of UV bright stars are already being observed in a cooperative effort between Service d'Aéronomie and Observatoire de Paris-Meudon.

4.2.2 Modelling

The SWAN instrument design is far from ideal for cometary studies. Furthermore, the default software for producing sky maps is optimized for maximal intensity conservation, trading off accurate representation of details. This is good for interstellar hydrogen distribution with smallest features in the range of five degrees, but much less suitable for comets. This justifies the use of a very simple model for estimating water production rates for most comets visible on SWAN maps. Significant advances in quality will only be achieved by simultaneously upgrading the model *and* the data processing utilities. Since the results obtainable with existing facilities are already valuable, the publishing of current results is made with the caveat that superior quality will be achieved later on when all the remaining issues are properly addressed.

There are many obvious improvements that can easily be incorporated to the current model and these have been already discussed in the previous chapter. The most important effects that are still absent are the Greenstein effect, radiation pressure, r and $\dot{r}$ dependence of lifetimes, and a rigorous treatment of branching ratios. There exists one less obvious improvement which is fairly important as well — time dependence of $Q_{\mathrm{H_2O}}$. It is not as

obvious in the context of a Haser model as the other modifications because usually Monte-Carlo type models are invoked to accommodate that as well as many other phenomena. However, it is relatively straightforward to modify the exospheric Haser model for time-dependent water production as outlined below.

Let us assume, neglecting the r dependence for the sake of brevity, that during some period $[0, T]$ the water production rate $Q_{\mathrm{H_2O}}$ varies in discrete steps as $\mathbf{q} = (Q_0, \ldots, Q_T)$. If we denote the local density at some distance R and solar angle θ from the nucleus given by a static Haser model by $n_H(\mathbf{q}, R, \theta) = \mathbf{q} \cdot \mathbf{h}(R, \theta)$ where $h_t(R, \theta)$ is some geometric function of its arguments and time t, then the column densities $\mathbf{n} = (N_0, \ldots, N_T)$ in the time-dependent case are

$$N_t(\mathbf{x}) = \sum_i H_{ti}(\mathbf{x}) Q_i \tag{4.1}$$

where the coefficients H_{ti} come from integrating the entity $h_t(R, \theta)\Theta_{ti}(R, \theta)$ where the distribution Θ_{ti} represents the contribution of $Q_{\mathrm{H_2O}}$ during the period $[i, i + 1]$ as observed at another time t. Such a construction can be used because the exosphere is collisionless by definition. Thus for a series of simultaneous observations at different parts of the coma

$$N_t(\mathbf{x}^j) = N_t^j = \sum_i H_{ti}^j Q_i \tag{4.2}$$

and the production rates can be formally solved as

$$\mathbf{q} = \mathbf{H}^{-1} \cdot \mathbf{n} \tag{4.3}$$

With proper choice of time steps the solution is well-behaving. Since SWAN observations are usually conducted with shorter time intervals than the relaxation time of the coma, it is possible not only to recreate a semicontinuous time series of $Q_{\mathrm{H_2O}}$ but also some uncertainties in the parametrization of the model can be fixed by the matching of overlapping time series from subsequent observations. The Θ_{ti} formalism makes this approch a *synchrone* model in contrast to a *syndyne* model (Keller and Meier, 1976). It

must also be remembered that in a realistic case it is not a trivial task to determine the Θ_{ti} distribution but once that has been accomplished, the rest of the analyzing process is quite straightforward.

4.2.3 Data processing

As has been mentioned before, the main scientific objective of the SWAN instrument is to observe variations in the cloud of interstellar hydrogen, and the standard data processing pathway has been optimized respectively. For the purpose of maximizing the gain from SWAN cometary data it is imperative that a parallel pathway gets established, addressing comet-specific issues as well as some other irregularities which have been detected. Until that, all SWAN results must be considered to be somewhat preliminary.

The necessary changes and additions to SWAN data processing pathway can be divided into three general categories: those, that address instrument related irregularities, then calibration issues, and finally those that relate to the reduction of the data themselves. The instrumental issues include, but may not be limited to

- LOS retrieval. The actuators display a hysteresis effect which currently limits LOS accuracy. This can be compensated by automatically detecting star positions as the mechanism sweeps back and forth, comparing them to known values and propagating the errors to other observations.

- SOHO rolls. At certain periods, the spacecraft has been rotating around its primary axis. The star tracking algorithm can only correct deviations which are of the order of some degrees. Thus, in the roll data the SOHO coordinates must be separately fixed into the range where star tracking can be used.

Calibration issues include:

- Long-term stability of sensors. Preliminary studies suggest that one sensor increases in sensitivity over initial months of observations and remains stable after that, but that the other sensor displays slowly

decreasing sensitivity. Based on the full sky maps, one can notice that the second sensor gets regularly exposed to either direct or reflected sunlight (the bright bar on the lower half of the sunward data gap) which might explain this behaviour.

- Absolute sensitivity for each sensor, including cross-calibration.
- Flatfielding and dark current compensation need more rigorous treatment as well.
- There are some results that suggest that a polarization effect takes place in the instrument, most likely caused by the mirrors in the periscope mechanism. This must be resolved as soon as possible.
- The degradation of sensors during the summer 1998 loss of SOHO. Besides sensitivity issues the changes in spectral response must also be addressed. This most likely requires a combined approach of modelling the changes in properties of the filter and comparing these to observations of stars whose spectra are well known.
- Spatial and temporal changes in the solar irradiation intensity, although not an instrumental effect, amount to 10–15% variation in water production estimates for comets and it is thus most desirable to compensate for this.

The calibration issues can mostly be solved through star observations although indirect measurements like comparing water production rates obtained by independent means can also be used to guide the process.

The current method of binning data by zeroth-order interpolation of observed pixel values pointwise projected to the grid coordinates is fine if the bin size is substantially larger than pixel size, and it has the desirable feature of conserving the signal intensity. Cometary observations seeking for spatial resolving power, however, will need this process in reversed form: bins should be projected to the pixel plate with correct area geometry and higher order interpolation. Ultimately, the concept of binning should be abandoned completely and the data reduction should be done for each

single 5×5 pixel observation separately, simultaneously achieving greater temporal resolution.

Currently the background elimination for the purpose of determining the water production rate of a comet is achieved through subtraction of two observations some time apart and then fitting the model for both appearances of the comet in the resulting difference image. The choice of dates to be subtracted is done by hand and a balance is sought between sufficient separation of comet locations and the amount of background variations. The obtained results, however, in some situations depend strongly on the choice of dates and great discretion is needed to judge the results. Besides the compensation of solar flux variation a more objective method for background removal is needed. Once the data processing enhancements mentioned in this section have been implemented, it will be relatively straightforward to automate this task so that not only two but several observations both before and after that in question are considered to determine the background signal level.

4.3 New initiatives

In the course of this work some new questions have arisen and some of them are mentioned here to give an example of future research which is based on but not limited to the current research topics. It is the humble opinion of the author that a certain "critical mass" has been achieved, after which the work in progress naturally spawns new ideas and topics for further research.

4.3.1 Ensemble properties

As described in paper 3, SWAN is producing a very large and consistent set of cometary L_α observations. Coverage over a wide range of heliocentric distances and comparison of observed comets will enhance our understanding of the correlation between Q_{H_2O} and visual magnitudes (Newburn, 1983, 1984; Roettger *et al.*, 1990; Jorda *et al.*, 1992) and other basic physical phenomena, like variability of hydrogen life time, as well. Preliminary analyses have suggested that short- and long-period comets occupy two different

domains in this respect. Also, two long-period comets, C/1996 Q1 Tabur and C/1997 N1 Tabur, appear to go through a near perihelion dissipation event similar to the one witnessed in the case of C/1999 S4 LINEAR (paper 5) and indeed, their Q_{H_2O} seem to be anomalously low relative to visual magnitude m_0 when compared to other long-period comets. Still, C/1996 N1 Brewington features even smaller water production rates without any apparent fragmentation. The topic clearly needs further evaluation.

4.3.2 Extended emission

The filtering method used to remove the background contribution from full sky images before they were fed to the neural network for the detection of comets as described in paper 2 had peculiar side effects with bright comets like C/1995 O1 Hale-Bopp. Instead of reducing them to a point-like source as with the stars, some comets reduced to a radial structure. When seeing that for the first time in November 1999 the author immediately dismissed it as a filtering effect and only when reading some literature on cometary dust jets the similarity of the structures invoked enough interest for a closer examination, which revealed that the initial guess had been true: the apparent "jets" were artificial features, most likely caused by the combined effect of less than instantaneous scanning velocity of the sensor head, and the coarse rebinning algorithm. However, when the filtering was made directly on the sensor pixels, one observing instance at a time, and the final image composed from the already filtered signal, a completely new discovery was made. The images of Hale-Bopp depicted a tail very much like the dust tail in appearance and location related to the anti-sunward direction but only in a scale of 10^7 km. This leftover hydrogen must come from an extended source — particles that dissipate far away from the nucleus — and independent observations on the O(^{1}D) line (Morgenthaler *et al.*, 1999), although restricted to the central one square degree around the nucleus, seem to confirm the case. This is a very interesting result and a new study is being initiated. The question about parent species remains open at this stage since it could be possible that the observed small deviation could represent emission from CHON particles.

4.3.3 Size distribution

The question about the size distribution of comets is an interesting one. The SWAN instrument has a sensitivity just on the verge of the interesting region and future initiatives for data processing may well yield some results. In this respect it will be most desirable to apply the full probabilistic treatment for cometary search which, despite being too slow for operational use, gives best possible detection sensitivity for a moderately small data set.

On the theoretical side, the three most obvious effects that depend on the size of the comet are the frictional force in the accretion region, solar and other irradiation effect possibly resulting in a complete degassing or destruction of a cometary body, and drag in penetrating collisions with giant molecular clouds (GMC). Treatment of the third effect, to the knowledge of the author, is left out in the literature since it is "negligible" in comparison with gravitational perturbations. That is certainly true for large comets but not necessarily so for smaller ones. A back-of-the-envelope (literally) calculation with default values for GMC and cometary bodies suggested that an average GMC is at least able to deplete the Oort cloud of particles up to centimeter sizes. A rigorous simulation should tell the true influence of this and whether it has some implications to cometary size distribution and thus to impact probability estimates. It must also be remembered that fragmentation of comets regularly replenishes the lower end of size distribution.

4.3.4 Solar flux

Moving farther away from pure cometary studies, the solar irradiation anisotropy mentioned in the calibration issues is from the viewpoint of cometary observations an unnecessary distraction to be removed if possible. This can be done by making a decomposition of the background field in both spatial and temporal domains. The part of the signal that describes the interstellar cloud lies in other spatial and temporal ranges than the signal from flux variations and the two can thus be separated. The usefulness of the variation field is not restricted to cometary studies, however, since it

can be inverted to obtain the original flux variation map *on the surface of the Sun*. Since SWAN sees almost 4π steradians of this illumination, the activity of the whole surface can be monitored. Qualitatively, the presence of an otherwise hidden active area has been predicted from this illumination (Bertaux *et al.*, 2000) but the advanced method will give quantitative results which complement those recently obtained by helioseismography (Lindsey and Braun, 2000).

Appendix A

Acronyms and nomenclature

A.1 Acronyms in the text

AANEAS Anglo-Australian Near Earth Asteroid Survey

AU Astronomical Unit, 1.496×10^8 km

BAO Beijing Astronomical Observatory, China

BSS Bigelow Sky Survey

CCD Charge Coupled Device

CHON organic particles, from **C**arbon, **H**ydrogen, **O**xygen, **N**itrogen

CLEAN an image restoration algorithm

CNSR Comet Nucleus Sample Return mission

CONTOUR Comet Nucleus Tour mission

CSS Catalina Sky Survey

DE Dynamics Explorer series satellite

DLR Institute of Planetary Exploration, Germany

ESA European Space Agency

FMI Finnish Meteorological Institute

FOS Faint Object Spectrograph on HST from 1990 to 1997

FOV Field Of View

GEO Geophysical Research Division of FMI

GHRS Goddard High Resolution Spectrograph on HST from 1990 to 1997

GMC Giant Molecular Cloud

HST Hubble Space Telescope, orbital astronomical platform

IAU International Astronomical Union

ICE International Cometary Explorer spacecraft

IHW International Halley Watch

IR infrared, electromagnetic radiation in the range 0.7–1000 μm

IRAS Infrared Astronomical Satellite

ISEE International Sun-Earth Explorer series spacecraft

ISO Infrared Space Observatory satellite

IUE International Ultraviolet Explorer satellite

JPL Jet Propulsion Laboratory of NASA

KAO Kuiper Airborne Observatory

L_α Lyman alpha resonant wavelength of neutral hydrogen at 121.6 nm

LASCO Large Angle and Spectrometric Coronagraph Experiment on SOHO

LIC Local Interstellar Cloud

LINEAR Lincoln Laboratory Near Earth Asteroid Research project

LONEOS Lowell Observatory Near-Earth Object Search

LOS Line Of Sight, instrument pointing direction

MCP Microchannel Plate photoelectron multiplier

MEM Maximum Entropy Method

NASA National Aeronautics and Space Administration, USA

NEA Near Earth Asteroid

NEAT Near Earth Asteroid Tracking program

NEO Near Earth Object

OAO Orbiting Astronomical Observatory series satellite

OCA Observatoire de la Côte d'Azur, France

ODAS OCA-DLR Asteroid Survey

OGO Orbiting Geophysical Observatory series satellite

PACS Palomar Asteroid and Comet Survey

PCAS Planet-Crossing Asteroid Survey

PSF Point Spread Function

PVO Pioneer Venus Orbiter spacecraft

$Q_{\mathrm{H_2O}}$ Water production rate, molecules per second

RLA Richardson-Lucy Algorithm

SA Service d'Aéronomie, France

SCAP Schmidt CCD Asteroid Program at BAO

SMM Solar Maximum Mission satellite

SOHO Solar and Heliospheric Observatory spacecraft

STIS Space Telescope Imaging Spectrograph on HST from 1997

SVD Singular Value Decomposition

SWAN Solar Wind Anisotropies instrument on SOHO

SWAS Submillimeter Wave Astronomy Satellite

TKS Three Channel Spectrometer on VEGA

UV ultraviolet, electromagnetic radiation in the range 10–400 nm

VEGA Venus-Halley spacecraft

WFPC Wide Field Planetary Camera, model 1 on HST from 1990 to 1993, model 2 since then

A.2 Comet naming convention

Historically, comets have received two different designations. Once found, the first designation was made up of the year of discovery followed by a lower case letter indicating the order within comet discoveries that year. Later, the comet received another designation with a year and a Roman numeral denoting the year and chronological order of perihelion passage. This naming convention had several shortcomings which were accentuated by the growing number of comet discoveries per year, and it was subsequently changed by IAU decision, starting from the beginning of 1995, to another one closer to naming convention of other minor bodies of the solar system. This work uses exclusively the new convention where the short-period comets are denoted by a number, indicating the order in which their periodicity was proven, and the letter P followed by the name of the comet (1P/Halley), and long-period comets have a sequence of the letter C and then year, letter and number denoting the year, half-month and a running

Table A.1: Comparison of new and old style designations of comets mentioned in this work.

New	Old provisional	Old final	Name
D/1770 L1		1770 I	Lexell
C/1959 Y1	1959k	1960 II	Burnham
C/1969 T1	1969g	1969 IX	Tago-Sato-Kosaka
C/1969 Y1	1969i	1970 II	Bennett
C/1973 E1	1973f	1973 XII	Kohoutek
C/1975 N1	1975h	1975 IX	Kobayashi-Berger-Milon
C/1975 V1	1975n	1976 VI	West
C/1978 T1	1978m	1978 XV	Seargent
C/1979 Y1	1979l	1979 X	Bradfield
C/1980 E1	1980b	1982 I	Bowell

number for the discovery followed by the name of discoverers or survey (C/1995 O1 Hale-Bopp). Comets which disappear have their P or C replaced by a D, e.g., 3D/Biela. The correspondence between designations of comets mentioned in this work is given in Table A.1. A utility for conversion between the old and new style notations is available at

`http://cfa-www.harvard.edu/iau/CometDes.html`

Appendix B

Data reduction

B.1 SWAN data levels

The current data processing pathway can be divided into discrete levels:

Level 0 This is the raw data coming from the spacecraft.

Level 1 The data are checked for gaps, irregularities and repeating sequences and divided into different files each containing one synoptic observing session. This is the basic level in which the data are stored for further analysis.

Level 2 Calibration and flatfielding is applied and instrument motor coordinates are converted to SOHO frame of reference coordinates.

Level 3 Observations are converted into the required coordinate system taking into account spacecraft location and attitude.

Level 4 Individual observations are binned into a map grid with ancillary information.

The current procedures transform the data from level 1 up to level 4 in one go. Because they are non-optimized development versions, large batches of

requests need long processing times. In the future, the alternative data processing path will work from level 1 up, correcting irregularities not properly addressed at the moment, and save the data on level 3 with ecliptic coordinates (J2000.0) as the default choice. This will make it feasible to query many observing sessions on the fly and the next generation of processing tools will completely sidestep the troublesome fourth level.

B.2 Processing utilities

This section documents some basic utilities developed by the author to process the data. All programming is done with IDL V5.3.

B.2.1 `ephcal.pro`

This program reads the orbital elements of a comet from a data file, solves the position of the comet in heliocentric ecliptic coordinates for the required period using basic procedures to obtain the true anomaly and then transforms the orbital plane to its actual orientation, and then calculates ephemerids for the known position of SOHO and creates a list of tabulated values for time, heliocentric and SOHO-centric distance and velocity of the comet, ecliptic longitude and latitude and motor coordinates and observing unit for SWAN command files. This is the operational utility used in planning comet specific observations and it has replaced an older and cumbersome amalgamation of old Fortran code and IDL frontend used during early operations. The orbital elements of C/1997 K2 were initially determined by driving this program with an *AMOEBA* type multidimensional optimizer algorithm and the result was quite adequate considering the inherent error margins although the convergence of the solution was very poor.

B.2.2 `zapper.pro`

This is an interactive preprocessing tool for the actual coma analyzer program `comod.pro`. Given two observations and an ephemeris file, the utility

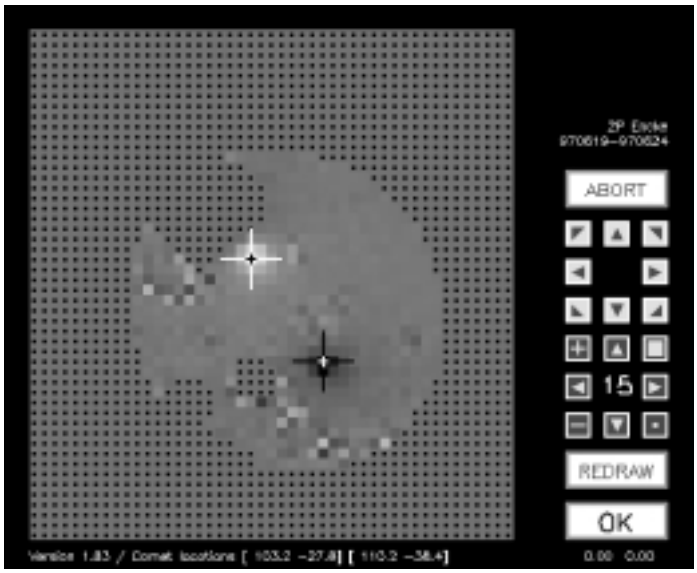

Figure B.1: Screengrab of `zapper.pro` in use. Two full sky observations containing an image of 2P/Encke have been framed for further processing.

locates the position of the comet in each observation and creates a composite frame of observations subtracted from each other containing both instances and selects an ellipse with the comet positions as foci for background determination. The user may then exclude pixels by painting over them with a mouse[1] and modify various parameters including estimated comet positions, ellipse size, location of the two observations relative to each other with subpixel stepping and coma peak search range. At the moment this tool is the most difficult among SWAN utilities to use properly and proper usage requires great discretion and some experience which nevertheless brings in some subjective influence. The situation is known

[1]It is necessary to exclude bright stars which do not completely cancel out because of pointing inaccuracies — otherwise they would affect the least squares fit of the comet model

to be less than ideal but without this utility the results would be even less reliable. This utility will become obsolete after the new processing path of SWAN data has been established, since at that point it will be fairly straightforward to implement a fully automated routine which uses the bulk of SWAN data to derive the background signal for all instances.

B.2.3 `comod.pro`

This is the program which determines the water production rate of a comet. Working on the preprocessed data from `zapper.pro`, the program calculates a subpixel model of the hydrogen coma for each instances of the comet with a reference $Q_{\mathrm{H_2O}}$ of 10^{28} s^{-1} and then does a least squares fit to the subtracted composite observation with locations of the coma, model multipliers and linear background coefficients as free parameters. Since the simple model used in this work is linear in $Q_{\mathrm{H_2O}}$ the multipliers yield the water production rate for each date right away.

Appendix C

Error estimation

Various possible sources of error have already been discussed elsewhere in this work. The topic has also been discussed in previous works (Bertaux *et al.*, 1998, 1999a) and the papers of this work discuss specific issues that are especially relevant in each case. The actual error bars are based on χ^2 values given by the *singular value decomposition* (SVD) method (Wilkinson and Reinsch, 1971) which is the preferred mathematical tool for solving (nearly) singular sets of equations. Because it is not as familiar as some statistical tools, a concise description of the method is given below.

C.1 SVD method

Any $M \times N$ matrix $\mathbf{A}$ for which $M \geq N$ can be written as the product of three matrices $\mathbf{U}$, $\mathbf{W}$ and the transpose of $\mathbf{V}$. $\mathbf{U}$ is a $M \times N$ matrix for which $\mathbf{U}^T\mathbf{U} = \mathbf{1}$, $\mathbf{V}$ a $N \times N$ matrix for which $\mathbf{V}^T\mathbf{V} = \mathbf{V}\mathbf{V}^T = \mathbf{1}$ and $\mathbf{W}$ a $N \times N$ matrix for which $W_{ij} = w_i\delta_{ij}$ where w_i, $i = 1, \ldots, N$ are the *singular values* of the matrix $\mathbf{A}$. A detailed discussion about the merits of this approach compared to other matrix inversion techniques is given in Press *et al.* (1986). It is sufficient to say here that the method readily diagnoses singular or nearly singular cases and provides an opportunity to figure out the best available solution. For the specific application of fitting

a combination of models to data the problem can be posed as:

Considering that there are M measurements $y_i = y(x_i)$ at abscissas x_i, and N models described by their corresponding functions X_j determining the *design matrix* $A_{ij} = X_j(x_i)$ of the problem, the fitting problem becomes equivalent to finding a vector $\mathbf{a}$ which minimizes

$$\chi^2 = |\mathbf{A} \cdot \mathbf{a} - \mathbf{y}|^2 \tag{C.1}$$

Applying SVD to $\mathbf{A}$ the solution can be immediately written as

$$a_j = \sum_i \sum_k \frac{U_{ik} y_k}{w_i} V_{ji} \tag{C.2}$$

and variance for each component of $\mathbf{a}$ is given by

$$\sigma^2(a_j) = \sum_i \left(\frac{V_{ji}}{w_i} \right)^2 \tag{C.3}$$

Here the components of $\mathbf{a}$ are linear coefficients of the corresponding models and thus $Q_{\mathrm{H_2O}} = a_q Q_{\mathrm{ref}}$ where a_q is the coefficient of the coma model and $Q_{\mathrm{ref}} = 10^{28}$ s^{-1} is the reference rate of the model.

The error estimates given by the SVD method are a combination of noise and other instrumental effects, and model inaccuracies. When subsequent error estimates of full sky and comet specific observations are compared with each other, it becomes apparent that model errors dominate the combination especially in cases where the comet is well above the background intensity level. It can therefore be anticipated that even higher quality results will be achieved with refined coma models.

Bibliography

A'Hearn, M. F., D. G. Schleicher, P. D. Feldman, R. L. Millis and D. T. Thompson, 1984. Comet Bowell 1980b. *Astron. J.* **89**, 579–591.

Alvarez, L. W., W. Alvarez, F. Asaro and H. V. Michel, 1980. Extraterrestrial cause for the Cretaceous-Tertiary extinction. *Science* **208**, 1095–1108.

Andrews, H. C. and B. R. Hunt, 1977. *Digital Image Restoration*. Prentice-Hall, London.

Asher, D. J. and D. I. Steel, 1998. On the possible relation between the Tunguska bolide and comet Encke. *Planet. Space Sci.* **46**, 205–211.

Ballard, D. and C. Brown, 1982. *Computer Vision*. Prentice-Hall, London.

Banaszkiewicz, M., S. Grzedzielski and C. Ruciński, 1989. On the possibility of detection of small comets in Ly-α. In *Physics of the Outer Heliosphere*, S. Grzedzielski and D. E. Page, eds., vol. 1 of *COSPAR Colloquia series*, pp. 97–100. Pergamon Press plc, Headington Hill Hall, England.

Bertaux, J.-L. and J. E. Blamont, 1970. Observation de l'émission d'hydrogène atomique de la comète Bennett. *C. R. Acad. Sci.* **270**, 1581–1584.

Bertaux, J.-L., J. E. Blamont and M. Festou, 1973. Interpretation of hydrogen Lyman-alpha observations of comets Bennett and Encke. *Astron. Astrophys.* **25**, 415–430.

Bertaux, J. L., J. Costa, T. Mäkinen, E. Quémerais, R. Lallement, E. Kyrölä and W. Schmidt, 1999a. Lyman-α observations of comet 46P/Wirtanen with SWAN on SOHO: H_2O production rate near 1997 perihelion. *Planet. Space Sci.* **47**, 725–733.

Bertaux, J. L., J. Costa, E. Quémerais, R. Lallement, E. Kyrölä, T. Summanen, T. Mäkinen and C. Goukenleuque, 1998. Lyman-alpha observations of comet Hyakutake with SWAN on SOHO. *Planet. Space Sci.* **46**, 555–568.

Bertaux, J. L., E. Kyrölä, E. Quémerais, R. Lallement, W. Schmidt, T. Summanen, J. Costa and T. Mäkinen, 1999b. SWAN observations of the solar wind latitude distribution and its evolution since launch. *Space Sci. Rev.* **87**, 129–132.

Bertaux, J. L., E. Kyrölä, E. Quémerais, R. Pellinen, R. Lallement, W. Schmidt, M. Berthé, E. Dimarellis, J. P. Goutail, C. Taulemesse, C. Bernard, G. Leppelmeier, T. Summanen, H. Hannula, H. Huomo, V. Kehlä, S. Korpela, K. Leppälä, E. Strömmer, J. Torsti, K. Viherkanto, J. F. Hochedez, G. Chretiennot, R. Peyroux and T. Holzer, 1995. SWAN: A study of solar wind anisotropies on SOHO with Lyman alpha sky mapping. *Solar Phys.* **162**, 403–439.

Bertaux, J. L., E. Quémerais, R. Lallement, E. Lamassoure, W. Schmidt and E. Kyrölä, 2000. Monitoring solar activity on the far side of the Sun from sky reflected Lyman α radiation. *Geophys. Res. Lett.* **27**, 1331–1334.

Biermann, L., 1968. JILA report. Tech. Rep. 93, University of Colorado.

Biermann, L. and E. Trefftz, 1964. Über die Mechanismen der Ionisation und der Anregung in Kometenatmosphären. *Z. Astrophys.* **59**, 1–28.

Biesecker, D. A., P. Lamy, O. C. St. Cyr, A. Llebaria and R. Howard, 1999. The sungrazing comets discovered with the SOHO/LASCO coronagraphs: 1996-1998. In *AAS/Division of Planetary Sciences Meeting*, vol. 31, p. 1404.

Biraud, F., G. Bourgois, J. Crovisier, R. Fillit, E. Gérard and I. Kazés, 1974. OH observations of comet Kohoutek (1973f) at 18 cm wavelength. *Astron. Astrophys.* **34**, 163–166.

Bowell, E. and K. Muinonen, 1994. Earth-crossing asteroids and comets: groundbased search strategies. In *Hazards due to Comets and Asteroids*, T. Gehrels, ed., pp. 149–197. University of Arizona Press, Tucson.

Boyarchuk, A. A., V. P. Grinin, A. I. Sheikhet and A. M. Zvereva, 1987. Pre- and post-perihelion Astron ultraviolet spectrophotometry of comet Halley: a comparative analysis. *Sov. Astron. Lett.* **13**, 92–96.

Boyarchuk, A. A., V. P. Grinin, A. M. Zvereva and A. I. Sheihet, 1986. Estimations of water production rate in the Halley comet using the ultraviolet data obtained on the space station 'Astron'. In *20th ESLAB Symposium on the Exploration of Halley's comet*, B. Battrick, E. J. Rolfe and R. Reinhard, eds., vol. 3 of *ESA SP-250*, pp. 193–194.

Brandt, J. C., M. F. A'Hearn, C. E. Randall, D. G. Schleicher, E. M. Shoemaker and A. I. F. Stewart, 1996a. On the existence of small comets and their interactions with planets. *Earth Moon Planets* **72**, 243–249.

Brandt, J. C., M. F. A'Hearn, C. E. Randall, D. G. Schleicher, E. M. Shoemaker and A. I. F. Stewart, 1996b. Small comets (SCs): An unstudied population in the solar system inventory. In *Completing the Inventory of the Solar System*, T. W. Rettig and J. M. Hahn, eds., vol. 107 of *ASP Conference Series*, pp. 289–297. Astron. Soc. Pacific, San Francisco.

Brandt, J. C. and M. B. Niedner, 1985. ICE mission to P/Giacobini-Zinner and P/Halley: an update. *Pub. Astron. Soc. Pacific* **97**, 894–895.

Brownlee, D. E., 1979. Interplanetary dust. *Rev. Geophys. Space Phys.* **17**, 1735–1743.

Buzdien, S. A., M. C. Festou and P. D. Feldman, 1994. Solar flux variability and the lifetimes of cometary H_2O and OH. *Icarus* **107**, 164–188.

Cameron, A. G. W., 1978. Solar accretion disk and planetary formation. In *Origin of the Solar System*, S. F. Dermott, ed., pp. 49–74. Wiley, New York.

Cameron, A. G. W., 1986. The impact theory for the origin of the Moon. In *Origin of the Moon*, W. K. Hartmann, R. J. Phillips and G. J. Taylor, eds., pp. 609–616. Lunar and Planetary Institute, Houston.

Carruthers, G. R., C. B. Opal, T. L. Page, R. R. Meier and D. K. Prinz, 1974. Lyman-α imagery of comet Kohoutek. *Icarus* **23**, 526–537.

Ceplecha, Z., 1994. Impact of meteoroids larger than 1 m into the Earth's atmosphere. *Astron. Astrophys.* **286**, 967–970.

Chapman, C. R. and D. Morrison, 1994. Impacts on the Earth by asteroids and comets: Assessing the hazard. *Nature* **367**, 33–40.

Chyba, C. F., 1991. Extraterrestrial amino acids and terrestrial life. *Nature* **348**, 113–114.

Code, A. D., T. E. Houck and C. F. Lilie, 1970. Comet Tago-Sato-Kosaka (1969g). *IAU Circ.* **2201**, 1.

Code, A. D., T. E. Houck and C. F. Lilie, 1972. Ultraviolet observations of comets. In *Scientific Results from the Orbiting Astronomical Observatory (OAO-2)*, A. D. Code, ed., NASA SP-310, pp. 109–114.

Code, A. D. and D. Savage, 1972. OAO: review of scientific results. *Science* **177**, 213–221.

Combes, M., V. I. Moroz, J. F. Crifo, J. P. Bibring, N. Coron, J. Crovisier, T. Encrenaz, N. Sanko, A. Grigoryev, D. Bockelée-Morvan, R. Gispert, C. Emerich, J. M. Lamarre, F. Rocard, V. Krasnopolsky and T. Owen, 1986. Detection of parent molecules in comet Halley from the IKS-Vega experiment. In *20th ESLAB Symposium on the Exploration of Halley's comet*, B. Battrick, E. J. Rolfe and R. Reinhard, eds., ESA SP-250, pp. 353–358.

Combi, M. R. and A. H. Delsemme, 1980. Neutral cometary atmospheres. I. An average random walk model for photodissociation in comets. *Astrophys. J.* **237**, 633–640.

Combi, M. R. and P. D. Feldman, 1992. IUE observations of H Lyman-α in comet P/Giacobini-Zinner. *Icarus* **97**, 260–268.

Combi, M. R., K. Kabin, D. L. DeZeeuw, T. I. Gombosi and K. G. Powell, 1997. Dust-gas interrelations in comets: Observations and theory. *Earth Moon Planets* **79**, 275–306.

Combi, M. R., A. A. Reinard, J. L. Bertaux, E. Quémerais and T. Mäkinen, 2000. SOHO/SWAN observations of the structure and evolution of the hydrogen Lyman-α coma of comet Hale-Bopp (1995 O1). *Icarus* **144**, 191–202.

Combi, M. R., A. I. F. Stewart and W. H. Smyth, 1986. Pioneer Venus Lyman-α observations of comet P/Giacobini-Zinner and the life expectancy of cometary hydrogen. *Geophys. Res. Lett.* **13**, 385–388.

Craven, J. D. and L. A. Frank, 1987. Atomic hydrogen production rates for comet P/Halley from observations with Dynamics Explorer 1. *Astron. Astrophys.* **187**, 351–356.

Craven, J. D., L. A. Frank, R. L. Rairden and M. R. Dvorsky, 1986. The hydrogen coma of comet Halley before perihelion: preliminary observations with Dynamics Explorer 1. *Geophys. Res. Lett.* **13**, 873–876.

Crovisier, J., 1989. The photodissociation of water in cometary atmospheres. *Astron. Astrophys.* **213**, 459–464.

Crovisier, J., K. Leech, D. Bockelée-Morvan, T. Y. Brooke, M. S. Hanner, B. Altieri, H. U. Keller and E. Lellouch, 1997. The spectrum of comet Hale-Bopp (C/1995 O1) observed with the Infrared Space Observatory at 2.9 AU from the Sun. *Science* **275**, 1904–1907.

Crovisier, J. and F. P. Schloerb, 1991. The study of comets at radio wavelengths. In *Comets in the Post-Halley Era*, R. L. Newburn, Jr., M. Neugebauer and J. Rahe, eds., vol. 1, pp. 149–173. Kluwer Academic Publishers, Dordrecht.

Delsemme, A. H., 2000. Cometary origin of the biosphere. *Icarus* **146**, 313–325.

Delsemme, A. H. and D. C. Miller, 1970. Physico-chemical phenomena in comets II. Gas adsorption in the snows of the nucleus. *Planet. Space Sci.* **18**, 717–730.

Delsemme, A. H. and D. C. Miller, 1971. Physico-chemical phenomena in comets III. The continuum of comet Burnham (1960 II): The differentiation of a short period comet. *Planet. Space Sci.* **19**, 1229–1257.

Delsemme, A. H. and D. A. Rud, 1973. Albedos and cross-sections for the nuclei of comets 1969 IX, 1970 II and 1971 I. *Astron. Astrophys.* **28**, 1–6.

Delsemme, A. H. and P. Swings, 1952. Hydrates de gas dans les noyaux cométaires et les grains interstellaires. *Ann. d'Astrophys.* **15**, 1–6.

Delsemme, A. H. and A. Wenger, 1970. Physico-chemical phenomena in comets I. Experimental study of snows in a cometary environment. *Planet. Space Sci.* **18**, 709–715.

DiSanti, M. A., U. Fink and A. B. Schultz, 1990. Spatial distribution of H_2O^+ in comet P/Halley. *Icarus* **86**, 152–171.

Dolginov, A. Z. and Y. N. Gnedin, 1966. A theory of the atmosphere of a comet. *Icarus* **5**, 64–74.

Donahue, T. M., T. I. Gombosi and B. R. Sandel, 1987. Cometesimals in the inner solar system. *Nature* **330**, 548–550.

Drake, J. F., E. B. Jenkins, J. L. Bertaux, M. Festou and H. U. Keller, 1976. Lyman-alpha observations of comet Kohoutek 1973 XII with Copernicus. *Astrophys. J.* **209**, 302–311.

Everhart, E., 1967. Intrinsic distributions of cometary perihelia and magnitudes. *Astron. J.* **72**, 1002–1011.

Feldman, P. D. and W. H. Brune, 1976. Carbon production in comet West 1975n. *Astrophys. J.* **209**, L45–L48.

Feldman, P. D., M. C. Festou, M. F. Ahearn, C. Arpigny, P. S. Butterworth, C. B. Cosmovici, A. C. Danks, R. Gilmozzi, W. M. Jackson, L. A. McFadden, P. Patriarchi, D. G. Schleicher, G. P. Tozzi, M. K. Wallis, H. A. Weaver and T. N. Woods, 1987. IUE observations of P/Halley - Evolution of the ultraviolet spectrum between 1985sep and 1986jul. *Astron. Astrophys.* **187**, 325–328.

Feldman, P. D., P. Z. Takacs, W. G. Fastie and B. Donn, 1974. Rocket ultraviolet spectrophotometry of comet Kohoutek (1973f). *Science* **185**, 705–707.

Feldman, P. D., H. A. Weaver, M. Festou, M. F. A'Hearn, W. M. Jackson, B. Donn, J. Rahe, A. M. Smith and P. Benvenuti, 1980. IUE observations of the UV spectrum of comet Bradfield (1979l). *Nature* **286**, 132–135.

Fernándes, J. A. and W. H. Ip, 1991. Statistical and evolutionary aspects of cometary orbits. In *Comets in the Post-Halley Era*, R. L. Newburn, Jr., M. Neugebauer and J. Rahe, eds., vol. 1, pp. 487–535. Kluwer Academic Publishers, Dordrecht.

Festou, M., E. B. Jenkins, H. U. Keller, E. S. Barker, J. L. Bertaux, J. F. Drake and I. Upson, W. L., 1979. Lyman-alpha observations of comet Kobayashi-Berger-Milon (1975 IX) with Copernicus. *Astrophys. J.* **232**, 318–328.

Festou, M. C., 1981. The density distribution of neutral compounds in cometary atmospheres I. Models and equations. *Astron. Astrophys.* **95**, 69–79.

Festou, M. C., P. D. Feldman, M. F. A'Hearn, C. Arpigny, C. B. Cosmovici, A. C. Danks, L. A. McFadden, R. Gilmozzi, P. Patriarchi, G. P. Tozzi,

M. K. Wallis and H. A. Weaver, 1986. IUE observations of comet Halley during the Vega and Giotto encounters. *Nature* **321**, 361–363.

Festou, M. C., H. U. Keller, J. L. Bertaux and E. S. Barker, 1983. Lyman-alpha observations of comets West 1976 VI and P/d'Arrest 1976 XI with Copernicus. *Astrophys. J.* **265**, 925–932.

Frank, L. A., J. B. Sigwarth and J. D. Craven, 1986. Comment on the paper 'On the influx of small comets into the Earth's upper atmosphere. II - Interpretation'. *Geophys. Res. Lett.* **13**, 701.

Gehrels, T., 1991. Scanning with charge-coupled devices. *Space Sci. Rev.* **58**, 347–375.

Grard, R., T. I. Gombosi and R. Z. Sagdeev, 1986. The Vega missions. In *Space missions to Halley's comet*, R. Reinhard and B. Battrick, eds., ESA SP-1066, pp. 49–70.

Greenstein, J. L., 1958. High-resolution spectra of comet Mrkos (1957d). *Astrophys. J.* **128**, 106–113.

Gull, S. F. and G. J. Daniell, 1978. Image reconstruction from incomplete and noisy data. *Nature* **272**, 686–690.

Hall, D. T. and D. E. Shemansky, 1988. No cometesimals in the inner solar system. *Nature* **335**, 417–419.

Haser, L., 1957. Distribution d'intensité relative dans une tête d'une comète. *Bull. Acad. Roy. Liège* **12**, 233–241.

Helin, E. F. and E. M. Shoemaker, 1979. Palomar planet-crossing asteroid survey, 1973-1978. *Icarus* **40**, 321–328.

Hildebrand, A. R., G. T. Penfield, D. A. Kring, M. Pilkington, A. Z. Camargo, S. B. Jacobsen and W. V. Boynton, 1991. Chicxulub crater: A possible Cretaceous/Tertiary boundary impact crater on the Yucatan peninsula, Mexico. *Geology* **19**, 867–871.

Högbom, J. A., 1974. Aperture synthesis with a non-regular distribution of interferometer baselines. *Astron. Astrophys. Supp.* **15**, 417–426.

Houpis, H. L. F. and D. A. Mendis, 1981. The nature of the solar wind interaction with CO_2/CO-dominated comets. *Moon Planets* **25**, 95–104.

Hoyle, F. and C. Wickramasinghe, 1981. Comets - a vehicle for panspermia. In *Comets and the Origin of Life*, C. Ponnamperuma, ed., pp. 227–239. D. Reidel Publishing Co., Dordrecht, Holland.

Huebner, W. F. and J. J. Keady, 1984. First-flight escape from spheres with r^{-2} density distribution. *Astron. Astrophys.* **135**, 177–180.

Huebner, W. F., J. J. Keady and S. P. Lyon, 1992. Solar photorates for planetary atmospheres and atmospheric pollutants. *Astrophys. Space Sci.* **195**, 1–289.

Huebner, W. F. and A. Weigert, 1966. Eiskörner in der Koma von Kometen. *Z. Astrophys.* **64**, 185–201.

Hughes, D. W., 1987. Cometary magnitude distribution and the fading of comets. *Nature* **325**, 221–232.

Hughes, D. W., 1990. Cometary absolute magnitudes, their significance and distribution. In *Asteroids, Comets, Meteors III*, C. I. Lagerkvist, H. Rickman, B. A. Lindblad and M. Lindgren, eds., pp. 327–342. Uppsala University, Uppsala, Sweden.

Irvine, W. M. and R. F. Knacke, 1989. The chemistry of interstellar gas and grains. In *Origin and Evolution of Planetary and Satellite Atmospheres*, S. K. Atreya, J. B. Pollack and M. S. Matthews, eds., pp. 3–34. University of Arizona Press, Tucson.

Irvine, W. M., S. B. Leschine and F. B. Schloerb, 1980. Thermal history, chemical composition and relationship of comets to the origin of life. *Nature* **283**, 748–749.

Jackson, M. W., J. Rahe, B. Donn, A. M. Smith, H. U. Keller, P. Benvenuti, A. H. Delseme and T. Owen, 1979. The ultraviolet spectrum of comet Seargent 1978m. *Astron. Astrophys.* **73**, L7–L9.

Jenkins, E. B. and D. W. Wingert, 1972. The Lyman-alpha image of comet Tago-Sato-Kosaka (1969g). *Astrophys. J.* **174**, 697–704.

Johnson, R. E., J. F. Cooper, L. J. Lanzerotti and G. Strazzulla, 1987. Radiation formation of a non-volatile crust. *Astron. Astrophys.* **187**, 889–892.

Jorda, L., J. Crovisier and D. W. E. Green, 1992. The correlation between water production rates and visual magnitudes in comets. In *Asteroids, Comets, Meteors 1991*, A. Harris and E. Bowell, eds., pp. 285–288. Lunar and Planetary Institute, Houston.

Kaneda, E., O. Ashihara, M. Shimizu, M. Takagi and K. Hirao, 1986. Observation of comet Halley by the ultraviolet images of Suisei. *Nature* **321**, 297–299.

Keller, H. U., 1973. Lyman-α radiation in the hydrogen atmospheres of comets. A model with multiple scattering. *Astron. Astrophys.* **23**, 269–280.

Keller, H. U., 1976. The interpretations of ultraviolet observations of comets. *Space Sci. Rev.* **18**, 641–684.

Keller, H. U., 1990. The nucleus. In *Physics and Chemistry of Comets*, W. F. Huebner, ed., chap. 2, pp. 13–68. Springer-Verlag, Berlin.

Keller, H. U., J. D. Bohlin and R. Tousey, 1975. High resolution Lyman alpha observations of comet Kohoutek (1973f) near perihelion. *Astron. Astrophys.* **38**, 413–416.

Keller, H. U. and R. R. Meier, 1976. A cometary hydrogen model for arbitrary observational geometry. *Astron. Astrophys.* **52**, 273–281.

Kissel, J. and F. R. Krueger, 1987a. The organic component in dust from comet Halley as measured by the PUMA mass spectrometer on board Vega 1. *Nature* **326**, 755–760.

Kissel, J. and F. R. Krueger, 1987b. Organic dust in comet Halley; and reply. *Nature* **328**, 117.

Kresák, Ľ., 1978. The Tunguska object: a fragment of comet Encke? *Bull. Astron. Inst. Czech.* **29**, 129–134.

Kresák, Ľ. and E. M. Pittich, 1978. The intrinsic number density of active long-period comets in the inner solar system. *Bull. Astron. Inst. Czech.* **29**, 299–309.

Krinov, E. E., 1963. The Tunguska and Sikhote-Alin meteorites. In *The Moon, Meteorites, and Comets*, B. M. Middlehurst and G. P. Kuiper, eds., pp. 208–234. University of Chicago Press, Chicago.

Kuiper, G. P., 1951. Origin of the solar system. In *Astrophysics*, J. A. Hynek, ed., pp. 357–424. McGraw Hill Book Co., New York.

Kumar, S., J. Holberg, A. L. Broadfoot and M. J. S. Belton, 1979. The Lyman-α observations of comet Kohoutek from Mariner 10. *Astrophys. J.* **232**, 616–623.

Lallement, R., P. Bertin, R. Ferlet, A. Vidal-Madjar and J. L. Bertaux, 1994. GHRS observations of Sirius-A, I. Interstellar clouds toward Sirius and Local Cloud ionization. *Astron. Astrophys.* **286**, 898–908.

Lemaire, P., C. Emerich, W. Curdt, U. Schühle and K. Wilhelm, 1998. Solar H I Lyman α full disk profile obtained with the SUMER/SOHO spectrometer. *Astron. Astrophys.* **334**, 1095–1098.

Lindsey, C. and D. C. Braun, 2000. Seismic images of the far side of the Sun. *Science* **287**, 1799–1801.

Linsky, J. L., A. Brown, K. Gayley, A. Diplas, B. D. Savage, T. R. Ayres, W. Landsman, S. N. Shore and S. R. Heap, 1993. Goddard high-resolution spectrograph observations of the local interstellar medium and deuterium/hydrogen ratio along the line of sight toward Capella. *Astrophys. J.* **402**, 694–706.

Lo Galbo, P., 1984. The Giotto spacecraft system and subsystem design. *ESA J.* **8**, 215–244.

Lucy, L. B., 1974. An iterative technique for the rectification of observed distributions. *Astron. J.* **79**, 745–754.

Lyttleton, R. A., 1948. On the origin of comets. *Mon. Not. Roy. Astron. Soc.* **108**, 465–475.

Lyttleton, R. A., 1953. *The Comets and their Origin*. Cambridge University Press, Cambridge.

MacQueen, R. M. and O. C. St. Cyr, 1991. Sungrazing comets observed by the Solar Maximum Mission coronagraph. *Icarus* **90**, 96–106.

Marsden, B. G., 1967. The sungrazing comet group. *Astron. J.* **72**, 1170–1183.

Marsden, B. G., 1989. The sungrazing comet group. II. *Astron. J.* **98**, 2306–2321.

McCoy, R. P., R. R. Meier, H. U. Keller, C. B. Opal and G. R. Carruthers, 1992. The hydrogen coma of comet P/Halley observed in Lyman α using sounding rockets. *Astron. Astrophys.* **258**, 555–565.

McFadden, L., D. J. Tholen and G. J. Veeder, 1989. Physical properties of Apollo, Aten and Amor asteroids. In *Asteroids II*, R. P. Binzel, T. Gehrels and M. S. Matthews, eds., pp. 442–467. University of Arizona Press, Tucson.

McFadden, L. A., M. F. A'Hearn, P. D. Feldman, H. Böhnhardt, J. Rahe, M. C. Festou, J. C. Brandt, S. P. Maran, M. B. Niedner, A. M. Smith and D. G. Schleicher, 1987. Ultraviolet spectrophotometry of comet Giacobini-Zinner during the ICE encounter. *Icarus* **69**, 329–337.

Meier, R. R., C. B. Opal, H. U. Keller, T. L. Page and G. R. Carruthers, 1976. Hydrogen production rates from Lyman-α images of comet Kohoutek (1973 XII). *Astron. Astrophys.* **52**, 283–290.

Morgenthaler, J. P., F. Scherb, C. W. Anderson, F. L. Roesler, R. J. Oliversen, N. E. Doane, W. H. Smyth and M. L. Marconi, 1999. The spatial distribution of O(^{1}D) in comet Hale-Bopp from 2,000 to 1×10^6 km. In *Proceedings of the American Astronomical Society Meeting*, vol. 194, p. 1501.

Moroz, V. I., M. Combes, J. P. Bibring, N. Coron, J. Rovisier, T. Encrenaz, J. F. Crifo, N. Sanko, A. V. Grigoryev, D. Bockelée-Morvan, R. Gispert, Y. V. Nikolsky, C. Emerich, J. M. Lamarre, F. Rocard, V. A. Krasnopolsky and T. Owen, 1987. Detection of parent molecules in comet P/Halley from the IKS-Vega experiment. *Astron. Astrophys.* **187**, 513–518.

Morrison, D., 1992. The Spaceguard Survey: Report of the NASA international Near-Earth-Object detection workshop. Tech. rep., JPL/NASA.

Mumma, M. J., H. A. Weaver, H. P. Larson, D. S. Davis and M. Williams, 1986. Detection of water vapor in Halley's comet. *Science* **232**, 1523–1528.

Neufeld, D. A., J. R. Stauffer, E. A. Bergin, S. C. Kleiner, B. M. Patten, Z. Wang, M. L. N. Ashby, G. Chin, N. R. Erickson, P. F. Goldsmith, M. Harwit, J. E. Howe, D. G. Koch, R. Plume, R. Schieder, R. L. Snell, V. Tolls, G. Winnewisser, Y. F. Zhang and G. J. Melnick, 2000. Submillimeter Wave Astronomy Satellite observations of water vapor toward comet C/1999 H1 (Lee). *Astrophys. J.* **539**, L151–L154.

Newburn, J., R. L., 1983. Modelling the neutral gas environment of comets with special application to P/Halley. *Adv. Space Res.* **2**, 111–120.

Newburn, J., R. L., 1984. A new calibration of the semi-empirical photometric theory for Halley and other comets. *Adv. Space Res.* **4**, 185–188.

Newton, I., 1687. *Philosophiae Naturalis Principia Mathematica*. Jussu Societatis Regis ac Typis Josephi Streater, London.

Oort, J. H., 1950. The structure of the cloud of comets surrounding the solar system, and a hypothesis concerning its origin. *Bull. Astron. Inst. Neth.* **11**, 91–110.

Opal, C. B. and G. R. Carruthers, 1977a. Carbon and oxygen production rates for comet Kohoutek (1973 XII). *Astrophys. J.* **211**, 294–299.

Opal, C. B. and G. R. Carruthers, 1977b. Lyman-alpha observations of comet West (1975n). *Icarus* **31**, 503–509.

Opal, C. B., G. R. Carruthers, D. K. Prinz and R. R. Meier, 1974. Comet Kohoutek: Ultraviolet images and spectrograms. *Science* **185**, 702–705.

Osborn, W. H., M. F. A'Hearn, U. Carsenty, R. L. Millis, D. G. Schleicher, P. V. Birch, H. Moreno and A. Gutierrez-Moreno, 1990. Standard stars for photometry of comets. *Icarus* **88**, 228–245.

Oxenius, J., 1965. Emission and absorption profiles in a scattering atmosphere. *J. Quant. Spectr. Radiat. Transfer* **5**, 771–781.

Oya, H., 1986. Japanese Halley missions with Sakigake and Suisei. *EOS Transact.* **67**, 65–66.

Parker, Q. A., M. Hartley, K. S. Russell and R. McNaught, 1990. The UK Schmidt Comet Search Initiative (SCSI) - First results. In *Asteroids, Comets, Meteors III*, C. I. Lagerkvist, H. Rickman, B. A. Lindblad and M. Lindgren, eds., pp. 413–416. Uppsala University, Uppsala, Sweden.

Press, W. H., B. P. Flannery, S. A. Teukolsky and W. T. Vetterling, 1986. *Numerical Recipes: The Art of Scientific Computing*. Cambridge University Press, New York.

Rabinowitz, D. L., 1991. Detection of Earth-approaching asteroids in near real time. *Astron. J.* **101**, 1518–1529.

Richardson, W. H., 1972. Bayesian-based iterative method of image restoration. *J. Opt. Soc. Am.* **62**, 55–59.

Roettger, E. E., P. D. Feldman, M. F. A'Hearn and M. C. Festou, 1990. Comparison of water production rates from UV spectroscopy and visual magnitudes for some recent comets. *Icarus* **86**, 100–114.

Ryan Jr., M. P. and I. G. Draganić, 1986. An estimate of the contribution of high energy cosmic-ray protons to the absorbed dose inventory of a cometary nucleus. *Astrophys. Space Sci.* **125**, 49–67.

Schleicher, D. G. and M. F. A'Hearn, 1988. The fluorescence of cometary OH. *Astrophys. J.* **331**, 1058–1077.

Schmidt, H. U., R. Wegmann, W. F. Huebner and D. C. Boice, 1988. Cometary gas and plasma flow with detailed chemistry. *Comp. Phys. Comm.* **49**, 17–59.

Schwehm, G. H., 1992. The Giotto Extended Mission to comet Grigg-Skjellerup - summary of preliminary results. *ESA Bull.* **72**, 61–65.

Sekanina, Z., 1982. The problem of split comets in review. In *Comets*, L. L. Wilkening, ed., pp. 251–287. University of Arizona Press, Tucson.

Sekanina, Z., 1984. Disappearance and disintegration of comets. *Icarus* **58**, 81–100.

Sekanina, Z., 1997. The problem of split comets revisited. *Astron. Astrophys.* **318**, L5–L8.

Sekanina, Z., P. Chodas and D. Yeomans, 1994. Tidal disruption and the appearance of periodic comet Shoemaker-Levy 9. *Astron. Astrophys.* **289**, 607–636.

Sekanina, Z. and D. K. Yeomans, 1984. Close encounters and collisions of comets with the Earth. *Astron. J.* **89**, 154–161.

Sheeley, N. R., Jr., R. A. Howard, M. J. Koomen and D. J. Michels, 1982. Coronagraphic observations of two new sungrazing comets. *Nature* **300**, 239–242.

Shoemaker, E. M., B. K. Lucchita, D. E. Wilhelms, J. B. Plescia and S. W. Squyres, 1982. The geology of Ganymede. In *Satellites of Jupiter*, D. Morrison, ed., pp. 435–520. University of Arizona Press, Tucson.

Shoemaker, E. M., P. R. Weissman and C. S. Shoemaker, 1994. The flux of periodic comets near Earth. In *Hazards due to Comets and Asteroids*, T. Gehrels, ed., pp. 313–335. University of Arizona Press, Tucson.

Shoemaker, E. M. and R. F. Wolfe, 1982. Cratering time-scales for the Galilean satellites. In *Satellites of Jupiter*, D. Morrison, ed., pp. 277–339. University of Arizona Press, Tucson.

Spahr, T. B., C. W. Hergenrother, S. M. Larson and H. Campins, 1996. High ecliptic latitude asteroid and comet survey with the Catalina Schmidt. In *Completing the Inventory of the Solar System*, T. W. Rettig and J. M. Hahn, eds., vol. 107 of *ASP Conference Series*, pp. 115–122. Astron. Soc. Pacific, San Francisco.

Stewart, A. I. F., 1987. Pioneer Venus measurements of H, O and C production in comet P/Halley near perihelion. *Astron. Astrophys.* **187**, 369–374.

Stokes, G. H., J. B. Evans, H. E. M. Viggh, F. C. Shelly and E. C. Pearce, 2000. Lincoln Near-Earth Asteroid program (LINEAR). *Icarus* **148**, 21–28.

Swings, P., 1941. Complex structure of cometary bands tentatively ascribed to the contour of the solar spectrum. *Lick Obs. Bull.* **19**, 131–136.

Turner, B. E., 1974. Detection of OH at 18-centimeter wavelength in comet Kohoutek (1973f). *Astrophys. J.* **189**, L137–L139.

Van Dishoeck, E. F. and A. Dalgarno, 1984. The dissociation of OH and OD in comets by solar radiation. *Icarus* **59**, 305–313.

Walker, R. G. and H. H. Aumann, 1990. IRAS comet observations - The continuing saga. *Adv. Space Res.* **10**, 151–158.

Wallis, M. K., 1980. Radiogenic melting of primordial comet interiors. *Nature* **284**, 431–433.

Watson, F. G., 1941. *Between the Planets*. Harvard University Press, Cambridge.

Weaver, H. A., P. D. Feldman, M. C. Festou, M. F. A'Hearn and H. U. Keller, 1981. IUE observations of faint comets. *Icarus* **47**, 449–463.

Weaver, H. A., M. J. Mumma, H. P. Larson and D. S. Davis, 1986. Post-perihelion observations of water in comet Halley. *Nature* **324**, 441–444.

Wegmann, R., K. Jockers and T. Bonev, 1999. H_2O^+ ions in comets: models and observations. *Planet. Space Sci.* **47**, 745–763.

Whipple, F. L., 1950. A comet model I. The acceleration of comet Encke. *Astrophys. J.* **111**, 375–394.

Whipple, F. L., 1951. A comet model II. Physical relations for comets and meteors. *Astrophys. J.* **113**, 464–474.

Wilkinson, J. H. and C. Reinsch, 1971. *Linear Algebra*, vol. 2 of *Handbook for Automatic Computation*. Springer-Verlag, New York.

Woods, T. N., P. D. Feldman, K. F. Dymond and D. J. Sahnow, 1986. Rocket ultraviolet spectroscopy of comet Halley and abundance of carbon monoxide and carbon. *Nature* **324**, 436–438.

Yamamoto, T. and O. Ashihara, 1985. Condensation of ice particles in the vicinity of a cometary nucleus. *Astron. Astrophys.* **152**, L17–L20.